

An Application of Aerial Drones in High Definition Mapping
for Autonomous Vehicles

by

Victoria Scherelis

A Thesis Presented to the
Faculty of the USC Graduate School
University of Southern California
In Partial Fulfillment of the
Requirements for the Degree
Master of Science
(Geographic Information Science and Technology)

December 2019

To my family

Table of Contents

List of Figures	vi
List of Tables	viii
Acknowledgements	ix
List of Abbreviations	x
Abstract	xi
Chapter 1 Introduction	1
1.1. Research Question and Objectives	1
1.2. Motivation	2
1.3. Study Sites	4
1.3.1. The Bertrandt Parking Lot	4
1.3.2. The German International School Parking Lot	5
1.4. Thesis Organization	6
Chapter 2 Related Work	8
2.1. Advancement Towards Autonomous Vehicles	8
2.2. Autonomous Vehicles in Parking Structures	10
2.3. Characteristics of High Definition Maps	10
2.4. Navigation Data Standard (NDS)	13
2.5. UAV Application in Remote Sensing	15
Chapter 3 Methods	16
3.1. Determination of Prototype HD Data Standards and Structure	18
3.2. Collection and Preparation of Drone Imagery	21
3.2.1. Bertrandt Parking Lot Data	22
3.2.2. German School Parking Lot Data	24
3.3. Manual Delineation of Required Features on Orthomosaics	26

3.4. Tool-based Extraction	29
3.4.1. Main Model.....	32
3.4.2. Extension Models.....	35
3.5. Validation Methods.....	39
Chapter 4 Results	40
4.1. Assessment of Drone-generated Images and Orthomosaics.....	40
4.2. Manual Delineation Results.....	47
4.3. Tool-based Extraction Results	50
4.4. NDS Conversion	57
Chapter 5 Discussion and Conclusion	60
5.1. Current HD Data Standards and the Drone-generated HD Datasets	60
5.2. Limitations and Challenges in Drone-based Data Collection.....	62
5.3. Proprietary Information	64
5.4. The Feature Extraction Processes	64
5.5. Future Research	67
5.6. Final Conclusions.....	69
References.....	70
Appendix A: Enlarged Version of the NDS Building Blocks	73
Appendix B: Questions and Answers from HERE Technologies	74
Appendix C: Bertrandt Parking Lot; Pix4D Quality Report.....	76
Appendix D: German School Parking Lot; Pix4D Quality Report.....	85

List of Figures

Figure 1 The Bertrandt parking lot: first study site.....	5
Figure 2 The German International School parking lot; second study site.....	6
Figure 3 Overview of the NDS building blocks	14
Figure 4 Thesis project workflow	16
Figure 5 Pix4D mapper output showing the flight path for the first study site	23
Figure 6 Pix4D mapper output showing the flight path for the second study site.....	24
Figure 7 Before (left) and after (right) snapshots of vegetation removal.	26
Figure 8 Illustration of boundary exclusion in manual delineation.	28
Figure 9 Illustration of the Multipart to Singlepart tool.	29
Figure 10 Main ArcGIS model: Orthomosaic to polygon feature classes	33
Figure 11 Bertrandt extension model: Polygon to line feature class	36
Figure 12 German school extension model: Polygon to line feature class	37
Figure 13 “Auto-Complete Polygon” tool demonstration.	38
Figure 14 Image overlap results. Study site 1 (left), study site 2 (right).	42
Figure 15 Bertrandt parking lot orthomosaic; study site 1	44
Figure 16 German School parking lot orthomosaic; study site 2.....	46
Figure 17 Manual delineation; final representation of study site 1.	48
Figure 18 Manual delineation; final representation of study site 2	49
Figure 19 Main model results for the Bertrandt study site 1	52
Figure 20 Bertrandt extension model results; final representation of study site 1.....	53
Figure 21 Main model result for the German School study site 2	55
Figure 22 German School extension model result; final representation of study site 2	56
Figure 23 Bertrandt parking lot in NDS format.....	58
Figure 24 German School parking lot in NDS format.....	59

Figure 25 Distortion in the northwest corner of the Bertrandt parking lot orthomosaic 63

Figure 26 Illustration of parking spot challenge from vehicles extraction 66

List of Tables

Table 1 Prototype HD data standards based on communication with Here, Inc.	19
Table 2 Prototype HD data structure for conversion to NDS	21
Table 3 Horizontal and vertical accuracy of ground control points.....	25
Table 4 Name and description of all geoprocessing tools applied.....	30
Table 5 Tool input parameters	31
Table 6 Time required for orthomosaic generation by Phantom 4 drone	41
Table 7 Summary of Pix4D processing results.....	41
Table 8 Error assesment calculated as the difference between initial and computed positions ...	43
Table 9 Time required for manual delineation	47
Table 10 Tool and model component runtime for tool-based extraction method.....	50
Table 11 Data collection by mapping-vehicles vs. by aerial drone	61

Acknowledgements

I sincerely thank my thesis advisor, Karen Kemp, Ph.D, for her continuous guidance and support. I would also like to thank Andrew Marx, Ph.D, and Robert Vos, Ph.D, for the advice and support that helped build the foundation for this research project, as well as Steve Fleming, Ph.D, for his participation on my thesis committee. Many thanks as well to my employer, Bertrandt Inc., who supported this research project in more ways than one. In particular, I would like to thank my mentors at Bertrandt, Inc., Lisa Gillman and Norman Timtschuk for their support and guidance that made this project possible. I am grateful for the information provided to me by HERE technologies and would like to thank Timm Kayser and Zaki Nassif Garcia for making that possible. Lastly, I would like to thank Andreas Pehlke from Bertrandt, Inc., for his continuous communication with me regarding NDS information and his efforts invested in this project by converting the outcomes to the NDS format.

List of Abbreviations

AAT	Automatic aerial triangulation
ADAS	Advanced driver-assistance systems
BBA	Bundle block adjustment
BMD	Basic map display
EPoSS	European technology platform on smart systems integration
GB	Gigabyte
GCP	Ground control point
GIS	Geographic information system
GISP	German International School of Portland
GSD	Ground sampling distance
GPS	Global positioning system
HD	High Definition
IMU	Inertial measurement unit
JSON	Javascript object notation
LiDAR	Light detection and ranging
NDS	Navigation data standard
TB	Terabyte
UAV	Unmanned aerial vehicle

Abstract

The future of the automotive industry continues to head towards the development of autonomous vehicles. Without a human driver behind the wheel, the self-driving vehicle must be able to navigate itself within the road network. This research project investigates the application of aerial drones, also known as unmanned aerial vehicles (UAVs), as an alternative data collection method to create HD datasets for use in autonomous vehicles. Drones may be a low-cost alternative method to the current leading data collection method of sensor-equipped mapping-vehicles. A Phantom 4 drone was used in two case studies to create orthomosaics of parking lots. The drone-generated orthomosaics were processed by methods of manual delineation and tool-based extraction to evaluate different methods of processing high-resolution data. In addition, current HD data standards were acquired from various sources to evaluate the results of the research project and to compare data collection methods. The results show that drone-based data collection with GPS correction techniques can be an accurate and low-cost alternative method. Both manual delineation and tool-based extraction techniques proved successful in extracting desired feature classes from the high-resolution imagery.

Chapter 1 Introduction

The future of the automotive industry heads towards self-driving, fully autonomous, vehicles. Many variables must be taken into consideration for autonomous vehicles to become a reality, such as the production of high-definition (HD) maps. To navigate autonomously within a road network, current maps within a vehicles' navigation system do not have the precision and accuracy needed to replace the driver's eyes on the road (Automotive World 2018). For example, most navigation systems symbolize the road driven as a single line segment, even if the line segment is a six-lane highway.

Semi-autonomous cars already exist and are bristling with sensors that help navigate the vehicle within a lane, however, these sensors only assist the driver and cannot replace the human behind the wheel (Hyatt 2018). To support these autonomous vehicles, high definition (HD) maps are built specifically for autonomous and semi-autonomous vehicles with high precision and detail and, ideally, centimeter level accuracy to ensure the vehicle stays within the lane (Vardhan 2017). Companies such as Here Inc., Lyft, and TomTom, among others, presently provide HD mapping services to the automotive industry by the use of sensor-equipped mapping vehicles (Kent 2015). These mapping vehicles may be the industry's leading mapping method; however, the services and sensors are expensive, and a driver is needed for every step of the way.

1.1. Research Question and Objectives

The main research question to be answered is: Can aerial drones be used as an alternative data collection method to provide drone generated imagery that can be used for the development of HD datasets for autonomous vehicles? The subsidiary research question to be answered is: What processing method of the drone-generated imagery renders the best results? To answer these questions, the objectives of this research study are to: (1) evaluate the accuracy and overall

quality of drone-generated orthomosaics from two case studies; (2) evaluate and compare manual and tool-based processing methods of drone-generated orthomosaics in the production of HD datasets; and, (3) compare the resulting datasets from the two case studies to current HD data standards in terms of the time required for data collection, the resulting data structure, and the quality and efficiency of data collection by means of aerial drones vs. traditional methods.

1.2. Motivation

Self-driving vehicles would not only allow the individual to lean back and relax while the auto-pilot chauffeurs, but it may lead to safer roads and a decline in automotive fatalities as well. According to the Insurance Institute for Highway Safety, 37,133 people died in motor vehicle crashes in the U.S in 2017 with a total of 34,247 crashes involving 52,645 vehicles (IIHS 2018). Globally, vehicle crashes account for 1.25 million deaths and 20 to 50 million injuries every year (CDC 2017). Handing the control over to the vehicle may reduce the amount of vehicle-related deaths as the computer in the autonomous vehicle does not experience human traits such as drowsiness or impairments due to drugs or alcohol. In 2016, 10,497 people died due to alcohol-impaired driving crashes, accounting for 28% of all traffic-related deaths in the United States (CDC 2019).

In addition to vehicle crashes due to impaired driving, a large percent of vehicle crashes are due to distracted driving habits. The distractions in the vehicles continuously grow as new technologies are introduced to the vehicles and as individuals use commuting time for additional activities such as eating food, watching movies, playing games, or texting on the cellphone. According to the U.S Department of Transportation, nine percent of U.S fatal crashes in 2016 were distraction-affected crashes, accounting for 3,450 deaths in motor vehicle crashes by distracted drivers (NHTSA 2018). Autonomous vehicles would make commuting time safer and

also more efficient as it would allow the individual to pay attention to other activities, all while the vehicle safely transports the individual to the destination.

Implementing a fleet of drones to create high definition maps for autonomous vehicles may also be beneficial to the environment. The mapping-vehicles used to create HD maps are required to drive each stretch of road multiple times to create high-quality data, burning fossil fuels in the process. Considering that the goal is to create an HD map network for all roads, the amount of fossil fuel burned to create such an HD road network comes with a cost to the environment. Instead of expanding our carbon footprint, drones with rechargeable lithium-powered batteries would be able to map without burning fossil fuel.

The production of an HD map network is also expensive. According to the artificial intelligence and industry review magazine Synced, the US rising star in HD mapping, DeepMap, charges \$5,000 per kilometer for its services in the US (Synced 2018). Creating a large HD map at such cost would require large investments by companies, most likely only attracting large companies that could afford it. Another option for smaller companies may be to create mapping-vehicles themselves, instead of paying for the services of other companies. As mapping-vehicles are bristling of sensors, structures to mount the sensors, and require high-processing powered computers and software, ultimately the cost of creating an HD map is still very high. Utilizing drones as an alternative HD mapping technique may save some money. A good quality drone such as the DJI Phantom 4 pro costs about \$1,500 brand new, according to the DJI sales website. In Germany, a vehicle often used for mapping purposes is the Volkswagen Passat (Dolgov and Thrun 2009). According to the VW sales website, a Passat costs about \$25,000 brand new. Even if all sensors would cost the same for the drone and the vehicle, the drone is still the more cost-efficient option.

1.3. Study Sites

The first steps taken in the autonomous vehicle network will occur within parking lots and highways, as these environments are less complex than city intersections and other fast-moving environments (Dokic et al. 2015). The introduction of autonomous vehicles will start slowly, with vehicles parking themselves in parking lots and vehicles driving down highways in auto-pilot. The two study sites chosen for this study are therefore two parking lots.

1.3.1. The Bertrandt Parking Lot

As the European automotive industry has great interest in HD map research, the engineering services company named Bertrandt supports this research study. To incorporate a parking structure in Germany, the first selected study site is the main parking lot of the Bertrandt company campus in Tappenbeck, Germany. Although the parking lot does not have lane separations, other components such as road (drivable surface), parking area, and parking spots (non-drivable surfaces) are included at this site. The Bertrandt parking lot is approximately 0.0183 km² (4.53 acres) and is located between fields and by residential houses (see Figure 1). Three ground control points were established from previously recorded benchmarks in the parking area. Due to Germany's very strict UAV guidelines and regulations, a drone flight was approved for a one-week window, January 7th-January 11th, 2019. The Bertrandt parking lot was utilized as one of two case studies to create a drone-generated map.

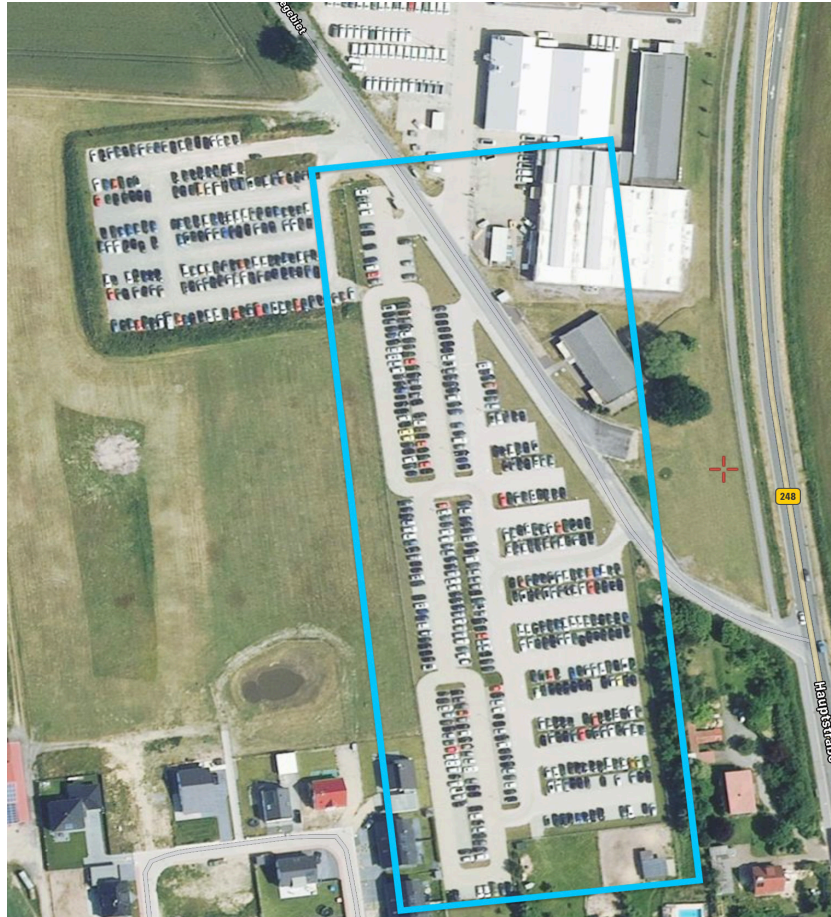


Figure 1. The Bertrandt parking lot; first study site. Source: satellites.pro

1.3.2. The German International School Parking Lot

The second case study was the parking lot of the German International School of Portland (GISP), located in Beaverton, Oregon (see Figure 2). The choice of location of the case studies was rather arbitrary, as long as the chosen study sites were parking lots and accessible to drone flights, they were suitable. Thus, the GISP parking lot was chosen due to the fact that the school is privately-owned, and the headmaster granted permission for drone flights of the property. The GISP parking lot was flown in May 2019 and is approximately 0.0106 km² (2.6 acres). To acquire the best absolute accuracy, four ground control points were set within the parking lot.

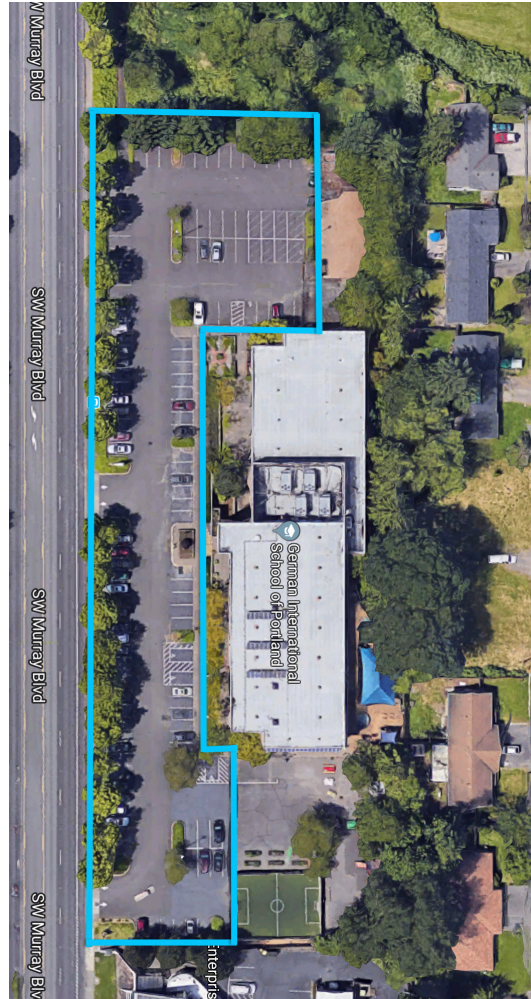


Figure 2. The German International School parking lot; second study site. Source: maps.google.com

1.4. Thesis Organization

This thesis includes four additional chapters. The next chapter provides a literature review to understand current advancements in the automotive industry and to give a background on high definition maps, their structure, and all they encompass. The next chapter also provides information on current UAV use as a remote sensing technique. Chapter 3 describes in detail the methods used to complete this research study, including the drone-generated data produced and used for orthomosaic generation, the feature extraction methods applied to the orthomosaics, and evaluation of the resulting datasets. Chapter 4 provides the results of the study. Chapter 5

discusses the conclusions drawn from the results, potential future research of this study, and also discusses any limitations faced.

Chapter 2 Related Work

As the automotive industry in Europe, China, and the US is particularly eager for the emergence of autonomous vehicles, abundant research has been done to explore the production of HD maps and autonomous vehicles. The current research, however, focuses heavily on HD map production by ground vehicles only. Other remote sensing methods, such as drones with imaging devices, can be used for map production as well and there is abundant research on their use within certain scientific fields, such as in agriculture and environmental sciences. This research study aims to bridge the gap between the production of HD maps for autonomous vehicles and the use of drones in certain scientific fields.

2.1. Advancement Towards Autonomous Vehicles

European automotive manufacturers and their suppliers have successfully introduced new smart components and systems, such as advanced driver assistance systems (ADAS), to the European high technology industry. ADAS are systems that help the driver in the driving process and include technological components such as collision avoidance, adaptive cruise control, and lane departure warning systems. These driver-assistant components have been technological breakthroughs within the automotive industry as they enabled road and passenger safety, energy efficiency, and emission reduction (Dokic et al. 2015).

According to the European Technology Platform on Smart Systems Integration (EPoSS), the introduction of autonomous vehicles is a feasible goal for the near future with milestones set at 2020, 2025, and 2030. By the first milestone of 2020, parking lot and traffic jam situations should be manageable by automated vehicles driving at low velocities. By 2025, highway autopilots should be introduced and by 2030 highly automated driving within cities with complex traffic structures will be possible (Dokic et al. 2015).

Besides the timeframe, different automation levels exist and range from level 0 (human driver has full control) to level 5 (fully autonomous vehicle) (Van Brummelen et al. 2018). As parking lot and traffic jam navigation are milestone 2020 goals, the automation level requirement is level 3 (conditional automation) in which the car is aware of its surroundings and can handle independently for a certain amount of time. This automation level can be found in the Tesla model X and S (Dokic et al. 2015; Van Brummelen et al. 2018). As the focus for the near future is on parking lots and traffic jams, the HD map generation of those parking lots will allow faster advancements of higher automation levels for navigation within parking structures.

Challenges facing the introduction of autonomous vehicles are many, as the higher-automation level requires more and better sensors on the vehicle, larger data storage space, and the maps must be upgraded frequently to provide sufficient information. A fully autonomous vehicle requires sensors such as sonar devices, stereo camera, lasers, radars, and highly accurate GPS to compare to the five human senses (Seif and Hu 2016). A LiDAR sensor would be an important sensor as it senses objects in the near-environment of the car with a high accuracy up to a range of 100 m and a rotational ability of 360 degrees. At a cost of \$4,000 per sensor, the LiDAR sensors are some of the most expensive sensors on the vehicle (Randall 2019). LiDAR sensors used by mapping-vehicles, such as the Velodyen top-end HDL-64E, retail at about \$100,000.

Besides the financial aspect of such expensive equipment, another challenge is the data collection from the sensors as one hour of drive time produces one terabyte of data and takes two days to process by high computing power (Synced 2018; Seif and Hu 2016). One solution to the current challenges of data collection, processing, and storage, is to consider all autonomous vehicles as part of the infrastructure of a future traffic system. This future traffic system would

consist of the autonomous vehicles, roadside units, HD maps, and high-performance computing and storage for cloud services (Seif and Hu 2016).

2.2. Autonomous Vehicles in Parking Structures

Current research in the field of autonomous driving focuses mostly on highly structured environments, such as highways or cities, or on unstructured environments, such as off-road driving. In highly structured environments, it is assumed that a topological graph, or lane-network graph, exists over the environment to which the vehicle is constrained to drive on with little to no deviations (Dolgov and Thrun 2009). For unstructured environments, the vehicle is not constrained to a topological graph and can freely choose a path, considering safety and other constraints. Parking structures fall in to the semi-structured category where a topological graph structure exists, but maneuvers off the graph are valid (Dolgov and Thrun 2009). Current research focuses on the use of topological graphs within these semi-structured environments to see if they benefit the vehicle in path planning or not. Results show that predetermined lane-networks (topological graphs) do, indeed, benefit the vehicle in path planning through a parking structure opposed to free-space path planning (Dolgov and Thrun 2009). For largescale multi-level structures such as parking garages, the approach of a predetermined path has also shown to be beneficial. In one study, based on surface maps of the corresponding environment and a calculated path through the parking garage, an autonomous vehicle was able to completely park itself within the parking garage (Kummerle et al. 2009).

2.3. Characteristics of High Definition Maps

Traditional maps used for navigation mainly serve visualization purposes and do not have the requirements needed for autonomous vehicles as they lack the accurate lane geometries (Massow et al. 2009). Maps particularly built for self-driving purposes are commonly referred to

as high definition maps or HD maps. These HD maps are extremely precise and contain a lot of information as the robots need precise instructions on how to maneuver within the 3D space (Vardhan 2017). To meet the need of higher quality maps, new HD map formats are emerging from mapping services companies such as TomTom and Here, Inc.. Some standardized map formats for specific companies already exist, such as the HD live map from Here and the highly automated driving (HAD) map from TomTom (Kent 2015; TomTom 2015; Massow et al. 2009).

Although HD map developers such as TomTom, Here, and Lyft, among others, are working towards a standardized format for all HD datasets, the exact format is currently still a fluid concept. The TomTom HD map consists of layers including lane models, traffic signs, road furniture, and lane geometry (TomTom 2018). Lyft, an on-demand transportation company, organized their HD map into five layers including the real-time layer, map priors layer, semantic map layer, geometric map layer, and the base map layer (Chellapilla 2018). The map priors layer shows locations where the behavior of objects (e.g. timing and sequence of traffic lights), people (e.g. bicyclists in the driving lane) and other vehicles (e.g. places where left turns are common) impact simple navigation decisions. The HD live map specifications from Here, Inc. structure the HD map into two major models known as the lane model (group 1) and road centerline model (group 2). These models are further split into a lane topology and geometry model (group 1), lane attribute model (group 1), link topology-geometry model (group 2), and road attributes model (group 2). The lane model from Here, Inc. is based on the topology of individual lanes, lane groups, and lane group connectors. It includes lane boundaries and lane paths as well as their lane-level attributes (Here 2018). The road centerline model is based on links and nodes, 2D geometry of polylines and shape points, and the attributes (Here 2018). With such differing

data structures and map specifications, an exact standard of the components an HD dataset must include has not yet been established.

Although the exact format specifications between HD datasets from different companies may still vary, all consider an HD dataset to comprise of multiple layers that place the vehicle precisely in a lane with information on road signs and markings in the vehicle's immediate surroundings. With varying data structures between different mapping and automotive companies, defining the data structure for an HD dataset is difficult.

To find common ground, a standard structure for the data would be ideal. As described in Massow et al. (2016), the infrastructure of an HD map can be generalized to contain three major layers consisting of 1) dynamic data, 2) road furniture data, and 3) road geometry data. The dynamic data includes up-to-date information on current incidents, hazards, and events such as construction areas or accidents (Massow et al. 2016). For example, the HD live map from Here, Inc. includes such a dynamic layer to receive up-to-date information in the vehicle by vehicle-to-vehicle communication. The idea of this communication technique is that all vehicles driving on the road are connected and inform each other of changes on the road (Bonetti 2016). The road furniture layer comprises of features that may influence the driver's behavior, such as road signs or traffic lights. Lastly, the road geometry layer contains detailed information about the absolute position of the road in general, as well as lane positioning and direction (Massow et al. 2016). With a dynamic map layer, the road geometry and road furniture layer do not have to undergo constant reconstruction, as general roadway structures do not change very often. This allows mapping companies to map a road for autonomous-vehicle-permitting purposes without constant re-mapping to record changes on the road.

2.4. Navigation Data Standard (NDS)

To standardize more than only the general structure of HD datasets, a navigation data standard (NDS) was developed by mapping companies, automobile manufacturers and their suppliers. The NDS format is a physical storage format of automotive-grade navigation data. The NDS consortium developed this standard with the aim to standardize navigation data for effortless exchange between different systems around the world (NDS association 2019). With a global data standard, the sharing of information and data would be instant and vehicles from various manufacturers would have the ability to be in constant connection. To make a global vehicle-to-vehicle connection and data standard a reality, automotive companies, suppliers, and mapping companies have joined the NDS Association. Members include Volkswagen, BMW, Daimler, Nissan, Hyundai, Mitsubishi electric, Bertrandt, Here technologies, TomTom, Garmin, Bosch, Panasonic, etc. (NDS Association 2019).

Described in detail in Chapter 27 of Winner et al. (2009), the uniqueness of the NDS format is the organization of data into so-called building blocks. The navigation database is first divided into update region databases. For example, Germany would be its own database. The update regions are further split in to components. The component databases are the building blocks. For example, the Germany database would include multiple unique databases such as the routing database and Basic Map Display (BMD) database. The USA database would include its own databases such as the routing and BMD database. The individual building blocks hold specific information of one kind, such as names, digital terrain models, or points of interests. Figure 3 provides an overview of the fourteen building blocks and their names. The data within the individual building blocks are in some form or another connected to the data within other

building blocks, where the most fundamental characteristic of the data is their coordinates and name (Winner et al. 2009).

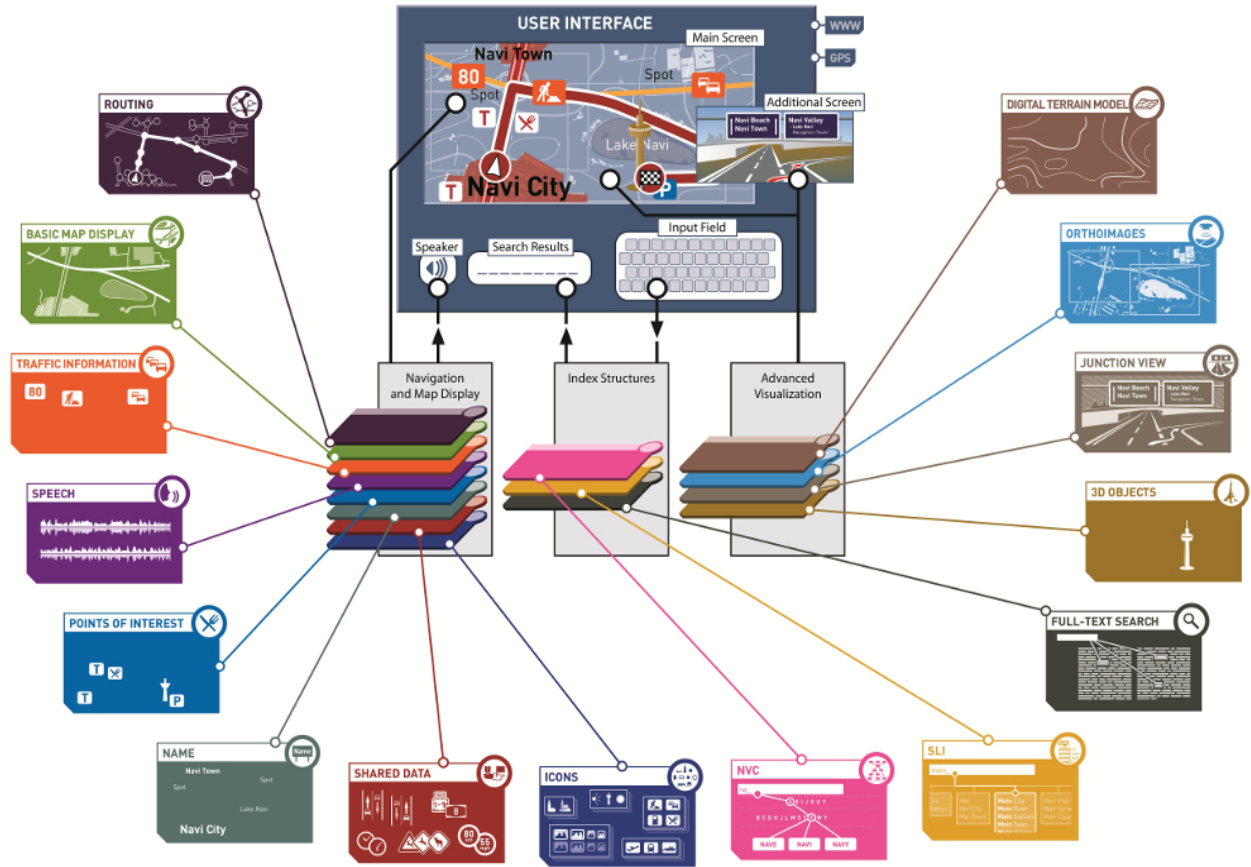


Figure 3. Overview of the NDS building blocks. An enlarged version of this Figure is included in Appendix A. Source: archive.is/WadYB (TomTom archives).

With extensive information on the data structure from the NDS format described in Winner et al. (2009), and the basic HD dataset structure described in Massow et al. (2016), the study described here focused on the Basic Map Display (BMD) database. Similar to the road geometry component described in Massow et al. (2016), the BMD building block includes areas, lines, and polygons of the absolute road position, parking lots, parking areas, and other basic components seen in a map. In other words, the BMD serves as a fundamental building block to which names, points of interests, and other building blocks are connected (Winner et al. 2009).

2.5. UAV Application in Remote Sensing

In recent years, drones have been used as an alternative remote sensing platform to satellites or aircraft in fields such as coastal and environmental science (Klemas 2015) as well as in agricultural sciences (Xiang 2011). UAVs have the ability to capture high resolution imagery suitable for ground measurements in both 2D and 3D flights (O'Neil-Dunne 2015), once the imagery is freed of distortions by software such as Pix4D. A recent study compared data collected from different DJI drones at different elevations, and the results show that data collected from DJI drones can be used for linear measurements, with an average margin of error of 1.1% for all flights. The results also show that flying at low altitudes of 66 feet (20 meters) improved measurement accuracy by 0.35%, with an average measurement error of only 0.26 feet (0.08 meters) for a phantom 4 pro DJI drone (Putch 2017). Although applied in multiple fields, the use of drones has yet to be applied to the production of HD maps for autonomous vehicles.

The benefits of UAVs for various applications include the ability to deploy a UAV relatively quickly and repeatedly at low altitude. With the miniaturization of sensors and the abundant availability of UAVs, they have become a versatile remote sensing platform (Laliberte 2016). As UAV applications have increased considerably in recent years, clearly, their application may extend to the automotive industry as an additional or alternative way to capture HD maps. This research explored that possibility.

Chapter 3 Methods

The objective of this research study was to evaluate the potential use of UAVs in HD mapping efforts to aid the implementation of autonomous vehicles in the near future. To investigate if UAVs are a viable alternative mapping method, several steps were taken before the study sites could be evaluated. The following workflow depicts all major steps taken to complete this research study (Figure 4). Dependencies within the workflow are shown by arrows, where each arrow starts from the dependent step and ends at the succeeding step.

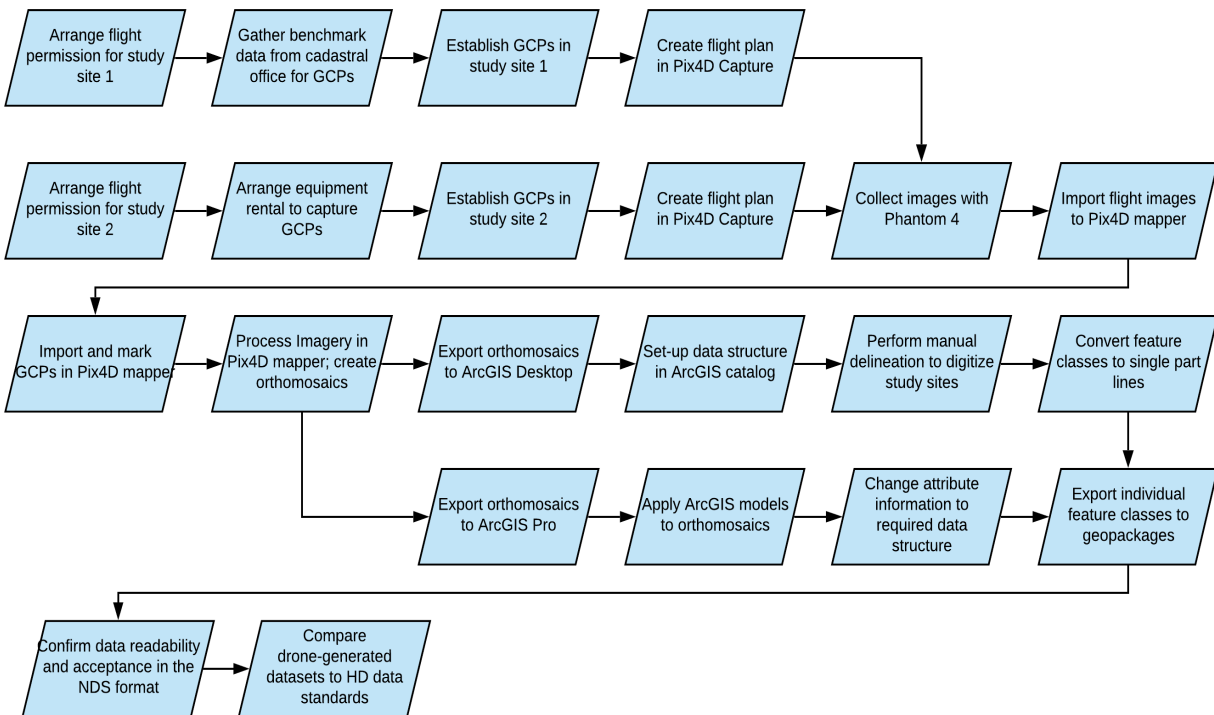


Figure 4. Thesis project workflow

In overview, the workflow proceeded as follows. As both the United States and Germany have specific regulations on the use and operation of drones, the selected study sites had to first be approved for flight. Flight approval took several months for the Bertrandt company campus in Tappenbeck, Germany, as image capture is prohibited on the property. On the other hand,

approval to fly over the German International School was readily obtained since it is private property and the school's owners were supportive of this research effort.

After flight approval, GCPs were established within the study sites to improve geolocation accuracy of the resulting orthomosaic. Pix4D capture was used to create flight plans for the study sites as this app allows route planning, locks in a specified altitude, and makes for easy transition to Pix4D mapper. Pix4Dmapper is a professional photogrammetry and drone-mapping software capable of orthomosaic generation based on orthorectification. According to the Pix4D support and training website, the drone images are not simply stitched together, instead the software computes keypoints in the images to find matches. After the initial matches are made, the software runs an automatic aerial triangulation (AAT) and bundle block adjustment (BBA). The orthomosaic is then created based on orthorectification which removes the perspective distortions from the imagery.

The drone imagery and GCPs were imported and processed through the initial processing step to compute keypoints and evaluate relative and geolocational accuracy errors. After initial processing, the third processing step was run to generate the orthomosaics. The orthomosaics were then exported for further use in ArcGIS Pro and ArcGIS Desktop. As described on the Esri website, both ArcGIS Pro and ArcGIS Desktop are mapping and analytics platforms to perform varying tasks on geospatial data. ArcGIS Desktop comprises of applications such as ArcMap, ArcCatalog, and ArcToolbox. ArcGIS Pro is the latest professional desktop GIS software that includes all applications in one, though since it is still evolving, it does not currently contain the entire set of functionalities built into the older ArcMap.

The exported orthomosaics underwent two independent processing methods in ArcGIS Desktop and ArcGIS Pro. These methods include manual delineation and tool-based extraction

of the orthomosaics, respectfully. After ArcGIS processing, the drone-generated HD datasets were exported to individual geopackages and compared to known HD data standards to evaluate the application of UAVs in HD mapping practices.

The following sections describe the work completed in detail.

3.1. Determination of Prototype HD Data Standards and Structure

The definition of an HD dataset is still fluid. However, the drone-generated datasets in this study needed to be compared to some sort of standard to validate the application of UAVs in HD mapping practices. Prototype HD data standards and data structure were thus compiled for this study by examining the research of related works, information on data specifications of HD datasets from the NDS consortium, and outreach to Here, Inc.

For logistical information on the production of HD datasets by mapping-vehicles, contacts from the US HAD Team at the HERE technologies mapping company agreed to answer several questions regarding the use of mapping-vehicles for the development of HD datasets. The answers from Here, Inc. provided this research study with a standard on the logistical aspects of the current leading method of HD map production: mapping vehicles. Based on these answers, Table 1 summarizes the prototype HD data standards used in this study as determined from the interview, including the questions that were asked, the answers, and answers found in related literature. The answers from Here, Inc. found in Table 1 have been summarized and are not the exact words from the contacts at Here, Inc. For the full unaltered answer, see Appendix B.

Table 1. Prototype HD data standards based on communication with Here, Inc.

Question to Here	Answer from Here	Information obtained by literature review	Prototype HD data standards
What is the geolocational accuracy of an HD map?	Absolute accuracy is below 1.0 m and for some features below 50 cm. The absolute accuracy is always higher than the relative accuracy and both are equally important.	Absolute accuracy of 1.0 m or below, in terms of x, y, z coordinates (Massow et al. 2009). Relative accuracy of 15 cm in terms of neighboring reference locations within the map and their relative position to each other (TomTom 2017).	Absolute accuracy must be below 1.0 m in term of x, y, z. Relative accuracy must be below the absolute accuracy.
How many times must the mapping vehicle drive a stretch of road to have sufficient data to create an HD map?	HERE True vehicles drive a map link only once. Re-drives occur if there is an indicator for change, such as construction.	A stretch is driven 5-10 times with a 64-channel LiDAR system (Synched 2019).	A stretch is driven 1-5 times to create an HD dataset. Drive frequency varies by company and their mapping vehicles.
What is the data volume obtained from driving a stretch of 1km?	Quite a lot, HERE True vehicles collect 60-80 Mbyte/second of raw data from lidar plus 80Mpixel imagery collected at 20 Hz. OEM vehicles collect 80-100 kbyte/km, OEM sensor data are segmented and highly compressed.	One hour of drive time corresponds to 1 terabyte (TB) of data (Seif and Hu 2016).	The data volume obtained is high, from 3-5 GB per minute to multiple TB per hour.
During data collection, how fast can the mapping vehicle go?	The speed is fairly low with a maximum speed of 80 km/h (49.7 mph). The faster the vehicle moves, the more sparse the lidar point cloud gets.	No related work found.	The maximum speed for a mapping vehicle is 80 km/h (49.7 mph).

Question to Here	Answer from Here	Information obtained by literature review	Prototype HD data standards
How much time, including processing time, is needed from data collection to the finished HD map that can be used by an autonomous vehicle?	Initial road mapping with HERE True raw sensor data takes several days, even weeks. Once initial mapping is done, meaning they consume already aggregated segmented content, the HAD team targets a 24hr-turnaround-cycle.	For a 20 km radius of a Beijing park, a fleet of mapping vehicles spent 5 days on fixed GPS and one day driving the stretch 5-10 times (Synched 2018). Processing 1 TB of collected data by means of high computing power requires two days to create usable navigation data (Seif and Hu 2016).	Initial processing time, from collection to completed HD dataset, takes several days to weeks.
Does an HD map of a parking lot exist? If so, what is the general data structure of the map?	The HAD team is focused on Limited Access Road network coverage, where physical dividers exists between roads. The area of “Parking” is not directly covered by HAD for now.	No related work found.	Currently, no publicly available HD map of a parking lot exists.
How much does the service of Here cost?	Here, Inc. cannot be hired as an individual contractor and thus cannot answer this question.	A mapping company named DeepMap charges \$5,000 per kilometer for its services in the US (Synched 2018).	Mapping companies for hire can charge sums of \$5,000 per kilometer for their services.

With the goal to obtain a uniform data structure, the NDS consortium requires all HD datasets to follow the same data structure. As described in Chapter 2, the NDS data structure constitutes multiple databases and multiple layers of geo-informational data. The focus of this research study was on the Basic Map Display (BMD) and the required NDS data structure of the BMD database. Based on the data structure used by Bertrandt, Inc. for conversion to NDS, Table 2 outlines the HD data structure used in this study for the drone-generated HD datasets. The digitized feature classes had to be drawn counter-clockwise as the NDS format can only display feature classes where the line-vertices are as such. Every feature class had to be exported to its own geopackage. A list with all feature class names used in the NDS format was provided by Bertrandt, from which the feature classes that occurred within the individual study sites were

selected. From there, the exported geopackages were converted to the NDS format by the engineering services company Bertrandt. Validation of the output of the workflow in this study is achieved if the data can be converted and displayed in the NDS format, such that the data can be displayed for use in autonomous vehicles.

Table 2. Prototype HD data structure for conversion to NDS.

Layer Name	Included features	Mandatory Attributes	Geometry
AREA_GREEN_URBAN	vegetation	fid, markCount, areaFeatureClass	Single part line
AREA_TRAFFIC_PARKING	the entire parking lot	fid, markCount, areaFeatureClass	Single part line
AREA_TRAFFIC_PARKING_LOT	parking spaces within the parking lot	fid, markCount, areaFeatureClass	Single part line
AREA_TRAFFIC_ROAD	road within the parking lot	fid, markCount, areaFeatureClass	Single part line
AREA_ROCK	landscaping made of rock	fid, markCount, areaFeatureClass	Single part line
BMD_LINES	borders, boundaries, fences, walls	fid, markCount, lineFeatureClass	Single part line

3.2. Collection and Preparation of Drone Imagery

As a remote sensing research project, data requirements for this study include drone-generated aerial imagery and a standard for comparison. The gathered data consisted of aerial imagery collected from a DJI Phantom 4 drone with one 12.4-megapixel camera that captured true color camera imaging at visible wavelengths. For both study sites, an orthomosaic was created and exported in a TIFF file format.

3.2.1. Bertrandt Parking Lot Data

A total of 413 images were collected at nadir and captured at an altitude of 15 meters (49 feet). This altitude was originally selected as it allowed for vehicle and tree canopy clearance at the study site while being low enough for detailed and clear imagery capture. The spatial resolution of the Bertrandt Parking lot was 0.57 cm per pixel. The images were collected during a period of continuous cloud cover to avoid glare and shadows in the images. As the battery life of a Phantom 4 drone allows a flight duration of approximately 30 minutes, several flights were flown to cover the entire study site. All images, including repeated flights, were imported and processed together as one project for each study site. Processing all imagery together allowed imagery from separate flights to be tied together and geolocated to one another.

Once all images were imported, GCPs were added to the project and marked manually within each image where they were visible. For the Bertrandt parking lot, previously measured benchmarks with an accuracy of 4 cm were available within the selected study site extent, made available by the cadastral office in Gifhorn, Germany. These benchmarks were used as GCPs and were marked on the ground with a large, high-contrast, target. A total of three GCPs were used for this study site. They are represented by blue crosses in the Pix4D mapper output shown in Figure 5. Here, all images used for the study site are represented as red dots, whereas the green lines illustrate the flight path of the drone while capturing the images.

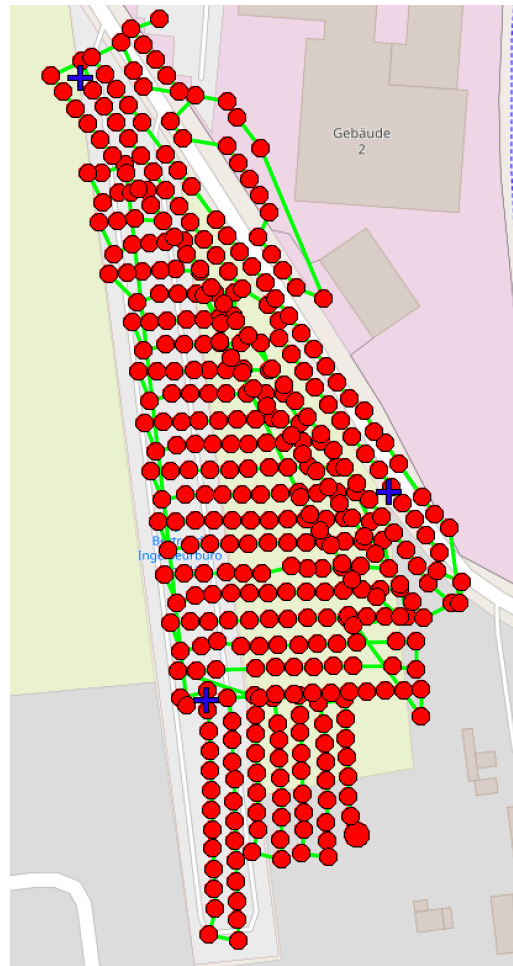


Figure 5. Pix4D mapper output showing the flight path (green lines), locations of captured images (red dots), and ground control points (blue crosses) for the first study site. The width of the mapped area shown is 120 meters.

After initial processing in Pix4D mapper, manual tie points (MTPs) were added as they can improve the reconstruction accuracy. Similar to GCPs, the MTPs can be marked in each image in which the selected tie point is visible. As the number of GCPs was relatively low for the size of this study site, a total of nine MTPs were added. After all desired points were marked, the project was reoptimized and reprocessed by rerunning the initial processing and orthomosaic generation steps in Pix4D mapper.

3.2.2. German School Parking Lot Data

A total of 454 images were captured with the Phantom 4 drone for the German School parking lot. The images were collected at nadir during light continuous cloud cover and at an altitude of 15 meters (49 feet). The spatial resolution of the German School parking lot was 0.62 cm per pixel. A total of 4 GCPs were evenly distributed throughout the study site, as shown in Figure 6.

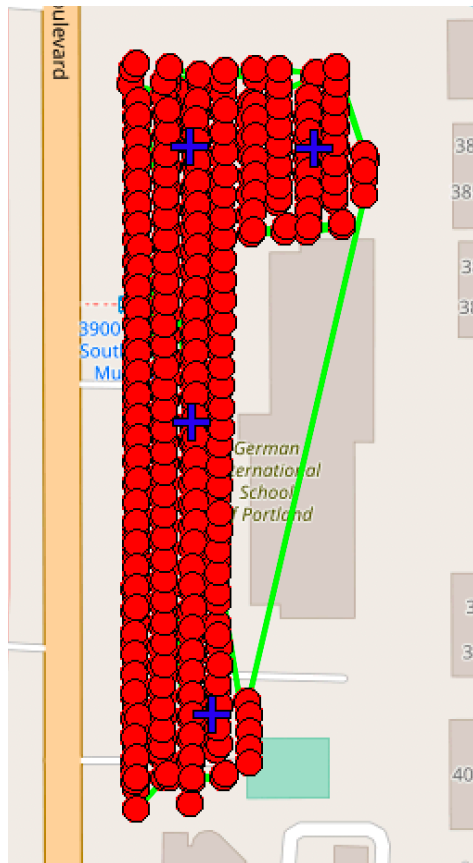


Figure 6. Pix4D mapper output showing the flight path (green lines), locations of captured images (red dots), and ground control points (blue crosses) for the second study site. The width of the mapped area shown is 100 meters.

As no previously measured benchmark data was available, the GCPs in study site 2 were established using a Trimble GeoExplorer XH 6000 series GPS unit, made available by the Spatial Science Institute at USC. As described by Trimble, the GeoXH handheld GPS unit uses

two multipath rejection technologies to provide decimeter, 10 cm, accuracy either real-time or after postprocessing (Trimble 2011). As shown in Table 3, submeter real-time horizontal accuracy and approximately one-meter vertical accuracy was achieved for all GCPs.

Table 3. Horizontal and vertical accuracy of ground control points.

	Horizontal Accuracy	Vertical Accuracy
GCP 1	0.69 m	0.87 m
GCP 2	0.77 m	0.93 m
GCP 3	0.74 m	0.99 m
GCP 4	0.64 m	0.86 m

The images for the German school parking lot were collected in May 2019, whereas the images for the Bertrandt parking lot were collected in January 2019. As a result, the orthomosaic generated for the German school parking lot encountered tree canopy obstruction above several parking spaces, due to the seasonal change to spring. To remove the overhanging vegetation, the generated orthomosaic was edited within the orthomosaic editor in Pix4D mapper. Within the editor, areas of the orthomosaic can be selected and subsequently all available images for that particular location are displayed. Multiple images shot from different angles or days can be selected to replace the image used with the obstructed view. Figure 7 shows the results of this removal of vegetation in the study site through the orthomosaic editor in Pix4D mapper. Once all edits were complete, the orthomosaic was saved and exported as the final orthomosaic for study site 2.



Figure 7. Before (left) and after (right) snapshots of vegetation removal.

3.3. Manual Delineation of Required Features on Orthomosaics

According to Bertrandt's efforts in converting data structures to NDS, current commercial efforts of HD dataset generation still depend heavily on the manual delineation of desired features. Thus, one of the two processing methods of the orthomosaics was done in ArcGIS Desktop and was comprised of the heads-up digitization of the study sites. The orthomosaics of both study sites were digitized following the required HD data structure.

In ArcCatalog, a geodatabase (.gdb) was established for each study site. Feature classes were created within the geodatabase for each feature class represented in the orthomosaic. For example, study site 1 had small landscaping areas of rock, thus an AREA_ROCK feature class was created in the geodatabase for study site 1. All areas, such as parking spaces or roads, were

initially set up as polygon feature classes. Borders, such as the end of the parking lot, were set up as a polyline feature class and labeled BMD_LINES, as shown in Table 3 above.

All feature classes within the geodatabase received the mandatory attributes of “markCount” and “line-” or “areaFeatureClass”. As Esri ArcGIS products assign every feature within a feature class a unique identifier known as OBJECTID, no additional “fid” attribute had to be entered as the OBJECTID was used as “fid.” The purpose of the markCount attribute was to show how many vertices a digitized feature has. All area features were required to contain a minimum of three vertices. The markCount attribute type was numeric and was calculated by the field calculator with the following python formula:

```
!shape!.pointcount
```

The line or areaFeatureClass was a text field and contained the name of the feature class, such as AREA_ROCK. Once the feature class data structure was established in ArcCatalog, the orthomosaic was digitized manually in ArcMap.

Since the NDS database can only read area feature boundaries where the line direction is counter-clockwise, all area feature classes were digitized counter-clockwise, tracing polygons over the orthomosaic from right to left. All tracing efforts were done within an editor session and saved periodically. For use in autonomous vehicles, individual parking space polygons cannot share a border with one another as the outer boundaries of each parking space must be unique. Curbs and other physical obstructions count as non-drivable surfaces and were therefore excluded in the tracing efforts, as shown in Figure 8. By excluding curbs, parking space lines, and other barriers, all polygons were given a unique boundary.



Figure 8. Illustration of boundary exclusion in manual delineation.

To convert the geopackages to the NDS format, all feature classes had to have a single part line geometry. Thus, once all tracing efforts were completed, the polygon feature classes were changed to polyline feature classes by use of the tool “Polygon to Line.” The tool converted the polygon boundaries to polylines. The new polylines were then used as inputs for the tool “Multipart to Singlepart,” a data management tool that separated the multipart polylines to single part lines. Figure 9 illustrates the change in geometry applied by use of the Multipart to Singlepart tool. With a single line geometry, the feature classes were in the correct format and

were exported as individual geopackages. Lastly, the geopackages were sent to Bertrand, Inc., to test if the data was NDS transferable.

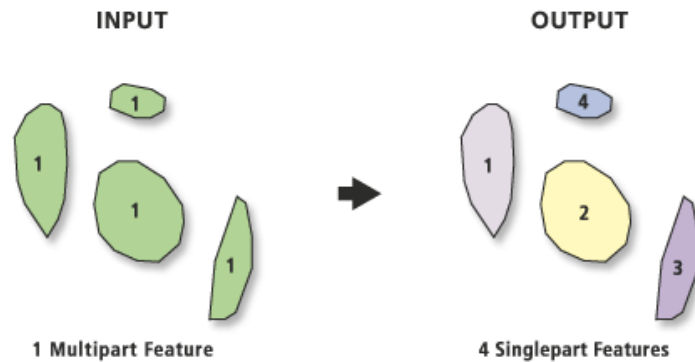


Figure 9. Illustration of the Multipart to Singlepart tool. Source: Esri 2019

3.4. Tool-based Extraction

The second processing method of the orthomosaic was done in ArcGIS Pro. The goal of this method was to create a tool-based model workflow that would automatically extract the desired features from the orthomosaic with little manual input by the user. To achieve this goal, object-based image classification and segmentation methods were applied based on Esri's object-oriented feature extraction workflow, Esri's post-classification processing workflow, and the Vector machine classification approach described in Tzotsos and Argialas (2008). The Vector machine classification approach used was a supervised classification method that has gained much attention due to its high classification accuracy and small needed training sets, according to Tzotsos and Argialas.

As shown in Figures 1 and 2, the raster inputs (orthomosaics) from the two selected study sites had very different spectral and spatial characteristics. The Bertrandt study site was made of cobble stone and parking spots were mostly occupied by vehicles of all colors and sizes. The German school study site had no vehicles within the orthomosaic and the dominant surface type was asphalt.

To accommodate the differences between the selected study sites, three ArcGIS models were developed. The main ArcGIS model included the processes applied to both study sites to extract the desired polygon feature classes from the raster input. Two extension models, labeled as the Bertrandt extension model and German school extension model, were created as the following processing tools varied due to the spectral and spatial differences between the study sites. The main ArcGIS model, combined with the extension model for the specified study site, rendered the final output of line feature class roads, parking spots, parking areas, and green areas. Table 4 shows a list of all the tools utilized in the three models and gives a brief description of each. Each of these models is explained in detail in the sections following.

Table 4. Name and description of all geoprocessing tools applied.

Tool Name	Tool Description	Tool Type
Extract by mask	Extracts raster cells which lay within the area defined by a mask.	Raster
Convolution smooth (5x5)	Smooths the raster with a 5-cell x 5-cell moving window by calculating the pixel value based on the weighs of its neighbors.	Raster
Segment mean shift	Groups together adjacent pixels that have similar spectral and spatial characteristics.	Raster
Train support vector machine classifier	A supervised classification method well suited for segmented images. The tool is a classification training tool and generates an Esri classifier definition file (.ecd).	Raster
Classify	Classifies a raster dataset based on a Esri classifier definition file and the raster inputs.	Raster
Reclassify	Reclassifies the values in a raster. Can be used to separate or join ranges of values.	Raster
Boundary clean	Smooths the boundaries between zones by changes regions of less than 3 cells.	Raster
Region group	Groups cells in a raster into regions where a unique number is assigned to each region. Individual regions are created for small pixel groups of the same value.	Raster
Select by attribute	Selects features by their specified attributes. A Clause is used to select certain attributes.	Raster/ Vector

Tool Name	Tool Description	Tool Type
Set null	Sets identified cell values to NoData. Setting a false null value is often used to change all values that meet specified conditions to NoData, or to create a mask.	Raster
Nibble	Replaces the cells in a raster, according to a mask, with the values of the nearest neighbors.	Raster
Raster to polygon	Converts a raster dataset to a polygon feature.	Raster
Eliminate	Removes small sliver polygons by merging them with the largest neighboring polygon.	Vector
Copy features	Copies specified features to a new feature class.	Vector
Buffer	Creates a buffer around a point, line, or polygon.	Vector
Erase	Creates a feature class that only has the portions of the input feature class that lie outside of the erase feature. In other words, it allows the area of one feature to be cut out of another feature.	Vector
Delete rows	Deletes all selected rows from the input.	Vector
Polygon to line	Convert a polygon feature to a line feature.	Vector
Multipart to singlepart	Separates multipart features into single part features.	Vector

Source: pro.arcgis.com

For some tools, optional parameters were entered to refine the output or to search for certain attributes. The “select by attribute” tool was used four separate times and was thus given a number for each tool use. Although mostly the same, a few parameters varied between study sites. Table 5 describes in more detail the tools’ parameters selected for the two study sites.

Table 5. Tool input parameters.

Tool	Input parameter study site 1	Input parameter study site 2																						
Segment mean shift	spectral detail: 20 spatial detail: 5 segment size: 30	spectral detail: 20 spatial detail: 5 segment size: 30																						
Reclassify	<table border="1"> <tr><td>0</td><td>1</td></tr> <tr><td>1</td><td>2</td></tr> <tr><td>2</td><td>3</td></tr> <tr><td>3</td><td>4</td></tr> <tr><td>4</td><td>1</td></tr> <tr><td>5</td><td>1</td></tr> <tr><td>6</td><td>3</td></tr> </table>	0	1	1	2	2	3	3	4	4	1	5	1	6	3	<table border="1"> <tr><td>0</td><td>1</td></tr> <tr><td>1</td><td>2</td></tr> <tr><td>2</td><td>3</td></tr> <tr><td>3</td><td>4</td></tr> </table>	0	1	1	2	2	3	3	4
0	1																							
1	2																							
2	3																							
3	4																							
4	1																							
5	1																							
6	3																							
0	1																							
1	2																							
2	3																							
3	4																							

Tool	Input parameter study site 1	Input parameter study site 2
Select by attribute 1	count < 10 000	count < 10 000 AND link ≠ 2 OR link = 2 AND count < 500
Select by attribute 2	shape area < 3	shape area < 3 AND gridcode ≠ 2
Select by attribute 3	(run 4x) gridcode = 1 gridcode = 2 gridcode = 3 gridcode = 4	(run 3x) gridcode = 1 gridcode = 2 gridcode = 3
Select by attribute 4	Not applicable	shape area < 5 OR shape length > 75
Buffer	0.3 m	Not applicable

3.4.1. Main Model

The main ArcGIS model, shown in Figure 10, depicts all geoprocessing tools used to extract polygon feature classes, along with their inputs and outputs. Dependencies within the model are shown by arrows, where each arrow starts from the dependent step and ends at the succeeding step. The model tools were color-coded where tools that require manual input are shown in blue.

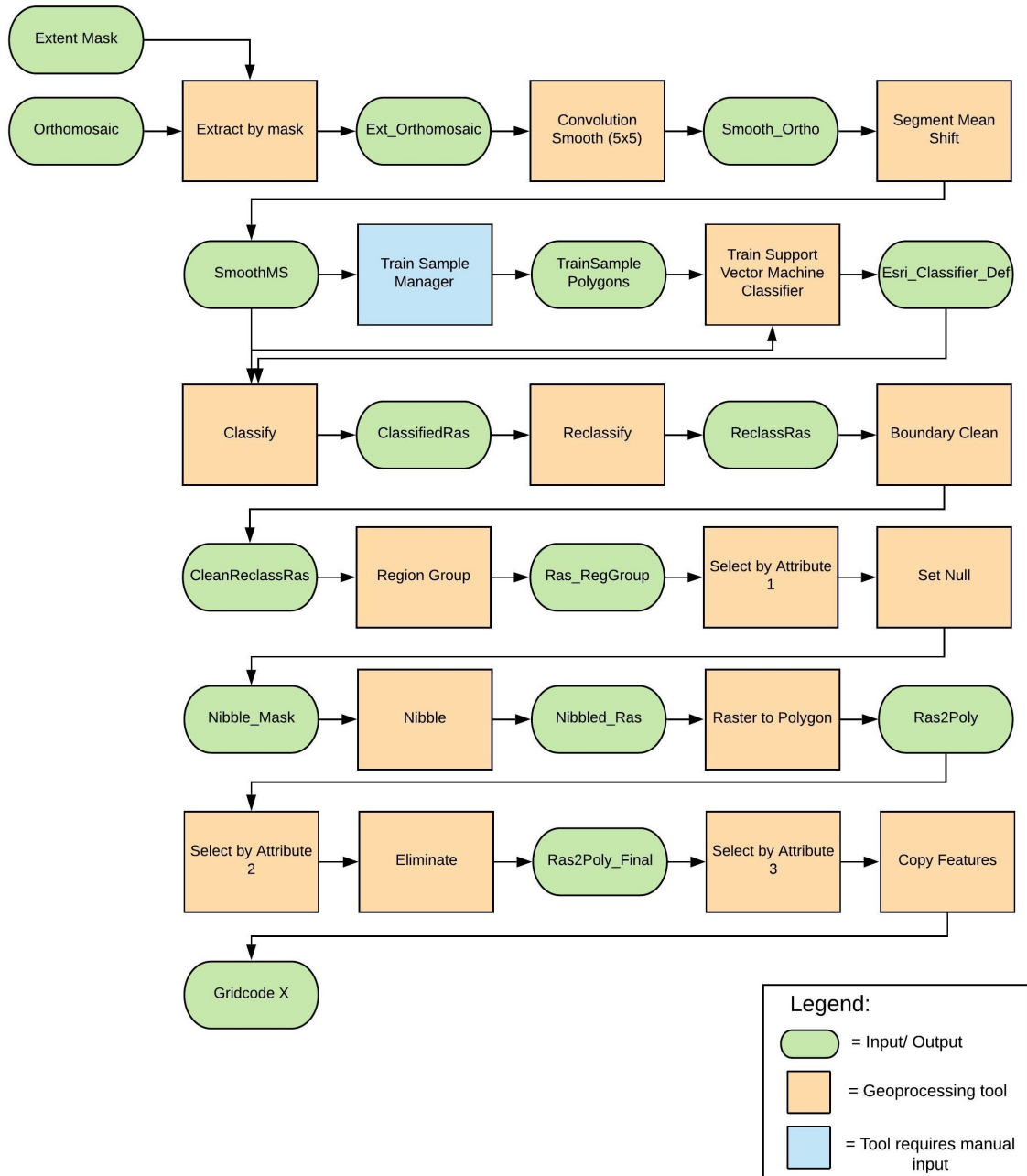


Figure 10. Main ArcGIS model: Orthomosaic to polygon feature classes

The initial model inputs were the orthomosaics exported from Pix4D mapper and a mask extent to reduce the size of the raster to the exact region of interest. The mask extent was created in an editor session. Once the extent was reduced and smoothed, the orthomosaic was segmented and then classified using training sample polygons created in the train sample manager, found in

the image classification pane. The training samples allowed for a supervised classification where samples are picked from the segmented image to represent a class value. For the Bertrand parking lot, training samples were taken for the road, parking area, vehicles, and green areas. For the German school parking lot, training samples were taken of the white-painted parking lines, road, sidewalks, and green areas. Although the sidewalk in the German school parking lot was not used in the final classification, training samples were created to ensure that sidewalks were not categorized with roads or other class values of significance.

After the raster was classified, new values were selected by the reclassify tool to group class values together as needed. The reclassify tool was important as the model may be run with different inputs and different training sample classes. After the reclassify tool, however, all class values are known, and similar classes are grouped together as one. In a high-resolution raster, small pixel regions can be classified incorrectly. To further process and regroup small pixel regions to the majority pixel class in its neighborhood, the remaining tools in the main model were based on the post-classification processing workflow from Esri. Boundaries between regions were cleaned and small pixel groups were removed from the classified raster by use of the tools Region Group and Nibble. Next, the raster was converted to a polygon feature class and small insignificant polygons were removed with the Eliminate tool. Lastly, the polygon feature class was exported to multiple polygon feature classes based on the class value attribute (Copy Features tool). With individual polygon classes produced for each desired feature, the work of the main ArcGIS model was complete and the separate extension models were applied to each study site for final processing.

3.4.2. Extension Models

The extension models include additional steps taken to extract line feature classes from each polygon feature class created by application of the main ArcGIS model. The class values, gridcode X, were subjected to various geoprocessing tools to render the final outputs.

Due to the vehicles present in the Bertrandt parking lot, a separate feature class was created for all vehicles within the parking lot and given the class value four. Parking spots were not marked with white lines, instead, individual cobble stones formed a striped pattern with slightly different spectral signatures to the surrounding cobble stones. To extract parking spaces, the vehicles within the parking spots were used to represent areas used for parking, instead of using the parking stripes. The vehicle feature class received a small buffer of 30 cm as vehicles are smaller than the allotted parking area.

Shown in Figure 11, the Bertrandt extension model received four inputs from the main ArcGIS model. After the vehicle feature class received a buffer, all polygon inputs were converted to polylines, followed by the conversion to single part lines. The final outputs of the extension model were again exported as geopackages and sent to Bertrandt, Inc., to test if the data was NDS transferable.

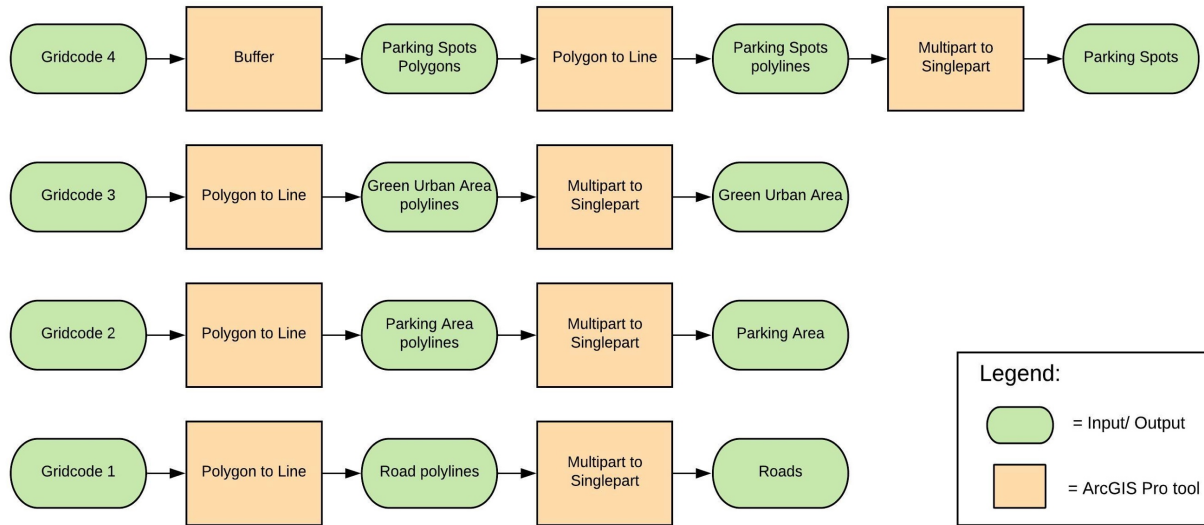


Figure 11. Bertrandt extension model: Polygon to line feature class

The German school extension model varied significantly from the Bertrandt extension model. Only three input features were rendered from the main ArcGIS model and additional geoprocessing tools were used on the three inputs, as shown in Figure 12. No vehicles were present in the German school parking lot during data collection, thus no feature class was created for the vehicles. As the parking lot was empty and parking lines were clearly marked, the parking line grid painted on top of the asphalt road was the focus point to create parking spaces.

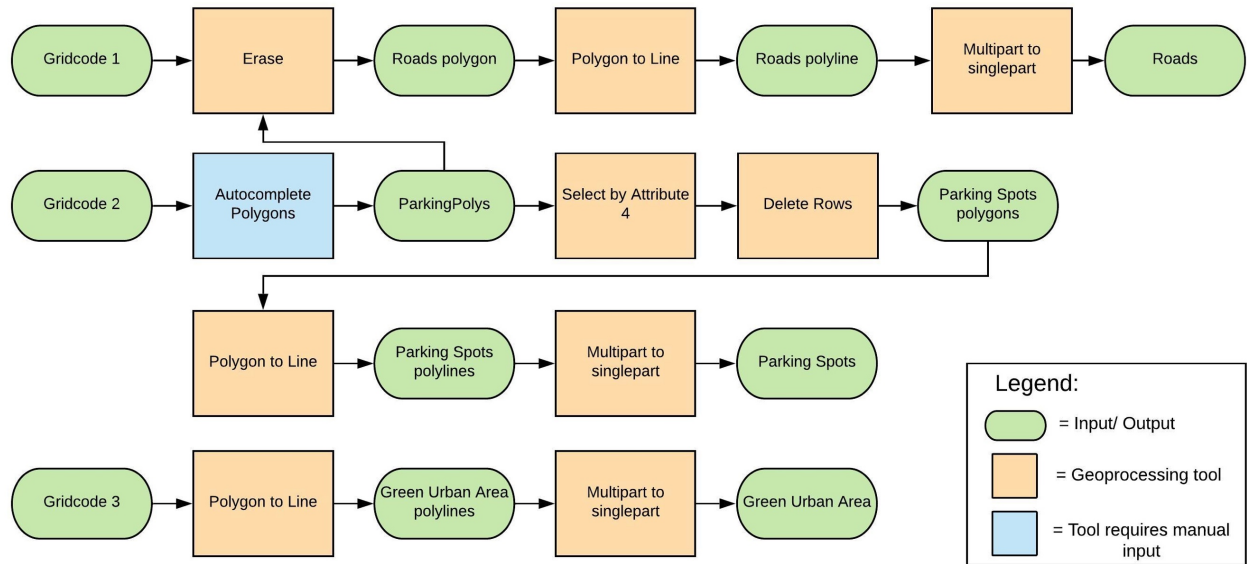


Figure 12. German school extension model: Polygon to line feature class

The German school parking lot required some manual input to create the rectangular parking spots. The parking line polygons, gridcode two, were used to create the parking spaces by use of the “Auto-Complete polygon” tool, available in an edit session when creating additional polygon features in a polygon layer. The autocomplete polygon created a new polygon by using the existing polygon’s geometry and the edit sketch to define the edges of the new polygon, as described on the Esri tool support website. In other words, the autocomplete polygon tool was used to quickly snap individual parking spaces on to the existing parking line grid. Figure 13 demonstrates the use of the autocomplete tool to create individual parking spaces.

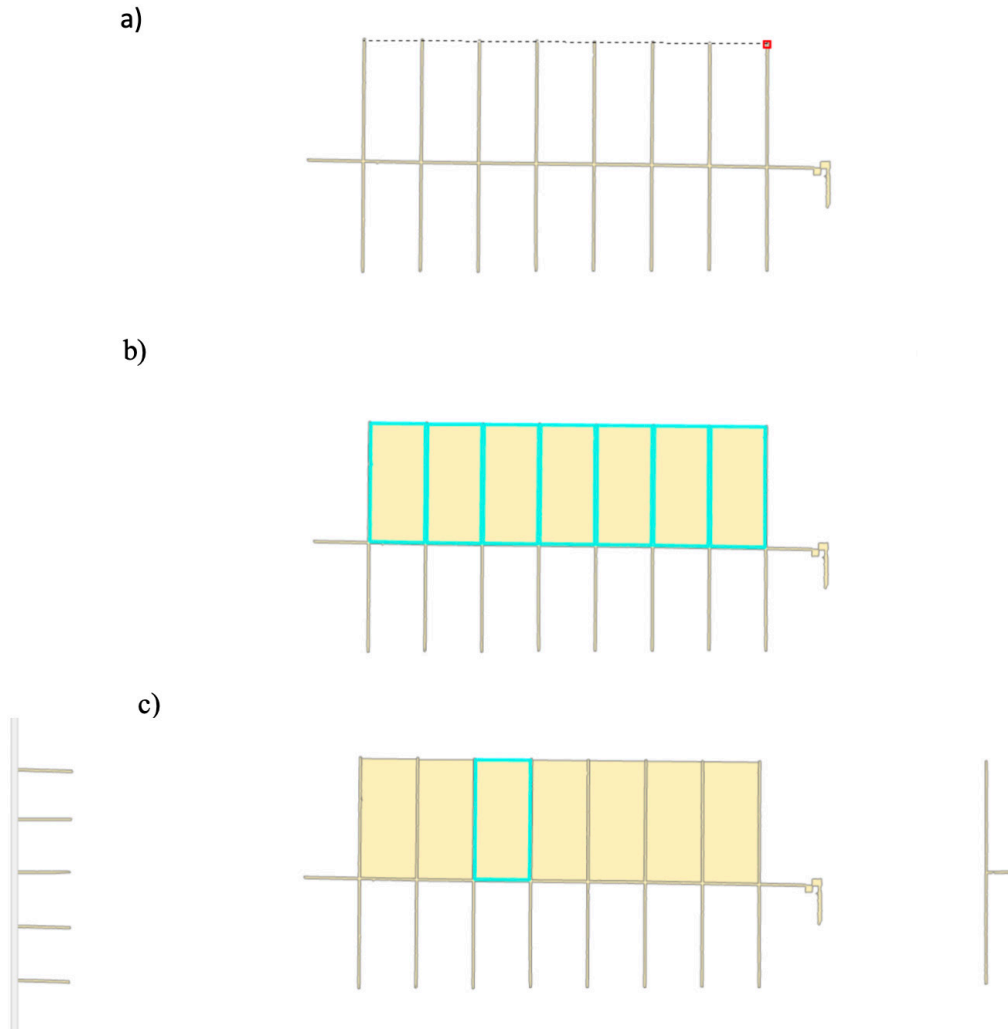


Figure 13. “Auto-Complete Polygon” tool demonstration. In step a) the user draws a line across the desired area where new polygons should be created. In step b) the polygons are created by double-clicking the mouse. Step c) shows one of the newly created polygon features outlined in blue.

Once all parking spaces were complete, the parking space polygons were used in conjunction with the road feature class to erase the road within the extent of the parking spaces. Due to an empty asphalt lot, the road polygon included all parking spaces, except for the white painted parking lines, as road. If exported as is, the parking spaces would have been categorized as drivable road. Thus, the erase tool was used to eliminate road within the extent of the parking area. As described in Section 3.3, all parking spaces required a unique boundary, so no two

parking spaces could share a line. The “delete rows” tool was therefore used on the parking area polygons to eliminate the white parking lines between the individual parking spaces. Lastly, all polygon feature classes were converted to single part polylines and exported as individual geopackages.

3.5. Validation Methods

The results of this research study include the drone-generated orthomosaics, the two HD datasets generated by manual delineation, and the two HD datasets generated by the application of various geoprocessing tools. The orthomosaics were evaluated based on accuracy, overall quality, and time. The quality of the orthomosaics and the collection process of drone imagery were the key components to answer the question if drones are a viable alternative mapping method. The accuracy was distinguished into absolute and relative accuracy. The absolute accuracy was defined by the x (east-west), y (north-south), and z (elevation) difference between the location of features on the orthomosaic and their true positions on the planet. The absolute accuracy of the drone-generated orthomosaic depended on the GCPs’ accuracy, distribution, and number. The relative accuracy is the positional accuracy of individual features on the map compared to the location of other features on the same map.

The four HD datasets generated by manual delineation and tool-based extraction methods were evaluated based on time of the processing method and data structure. The drone-generated HD datasets and the prototype HD data standards were compared to analyze if the drone-generated HD datasets matched the prototype HD standards. Lastly, HD datasets were sent to contacts at Bertrandt, Inc. to see if the data structure and quality was good enough to convert the HD datasets in to the NDS file format and could be displayed in the NDS database inspector.

Chapter 4 Results

This chapter presents the key findings of this research study. The UAV-based remote sensing technique applied in this study showed that high quality orthomosaics can be generated from low cost recreational drones with utilization of ground control points (GCPs). The orthomosaic processing method of manual delineation tested in this study shows successful conversion and display of the digitized objects in the NDS format. The tool-based extraction method, which included object-based image classification and post-processing methods, was successful in segmenting and classifying the orthomosaic and extracting the desired features. The tool-based extraction method was successfully converted to the NDS format but was not able to be displayed in the NDS database. The manual delineation processing method was therefore deemed the best practice for HD dataset development in this research study.

4.1. Assessment of Drone-generated Images and Orthomosaics

The imagery of the Bertrandt study site and German school study site were collected by a Phantom 4 drone with a 12.4-megapixel camera. The time invested in data collection consisted of flight planning, data collection, and processing in Pix4D mapper. Table 6 shows in detail the time taken for each step to generate the final orthomosaics. Once permission for drone flight was approved, the total time for data collection was approximately 11 hours for the Bertrandt study site and approximately 7 hours for the German school study site. The Bertrandt study site required multiple flights as the battery life of a Phantom 4 drone is 30 minutes. The Bertrandt study site included two separate flights where each flight heavily overlapped imagery from the previous flight. The German school study site was flown twice where each flight was 11 minutes and 10 seconds.

Table 6. Time required for orthomosaic generation by Phantom 4 drone.

	Bertrandt Study Site 1	German School Study Site 2
Allotted time for data collection	6 days	14 days
Time for flight planning	8 hrs	5 hrs
Total flight time	58 min 46s (2 flights)	22 min 20s (2 flights)
Time for initial image processing	1 hr 06 min 11s	45 min 02s
Time for Orthomosaic generation	32 min 31s	29 min 56s

All drone-collected images were processed in Pix4D mapper which produces extensive quality reports after initial processing. All quality results presented in this chapter were drawn from these reports. The complete quality reports summarized in this chapter can be found in Appendix C for study site 1 results and Appendix D for study site 2 results.

A summary of the processing results is shown in Table 7. Here, the ground sampling distance (GSD) is measured as the distance between two adjacent pixel-centers. The smaller the GSD, the greater the spatial resolution of the image. For both study sites, a sub-centimeter ground sampling distance was achieved.

Table 7. Summary of Pix4D processing results.

	Bertrandt Study Site 1	German School Study Site 2
Ground sampling distance (GSD)	0.56 cm (0.22 inches)	0.62 cm (0.24 inches)
Orthomosaic Resolution	0.57 cm/pixel	0.626 cm/pixel
Median matches per calibrated image	12795.6	3520.87
Area Covered	0.0184 km ² (0.0071 sq. miles)	0.0091 km ² (0.0035 sq. miles)
Ground control points (GCPs)	3	4
Manual tie points (MTPs)	9	0
Image Overlap	High (5+)	High (5+)

The number of image overlap ranges from 1 (low) to 5 (high), where low image overlap may give poor results. The number of overlapping images is computed for each pixel in the orthomosaic. Good results were generated for both study sites as most of the orthomosaics had high overlap with sufficient number of keypoint matches. Figure 14 shows the image overlap throughout the orthomosaics in both study sites. Low overlap can be seen along the edges of the orthomosaic, in particular for study site 1 where the flight extent was very restricted.

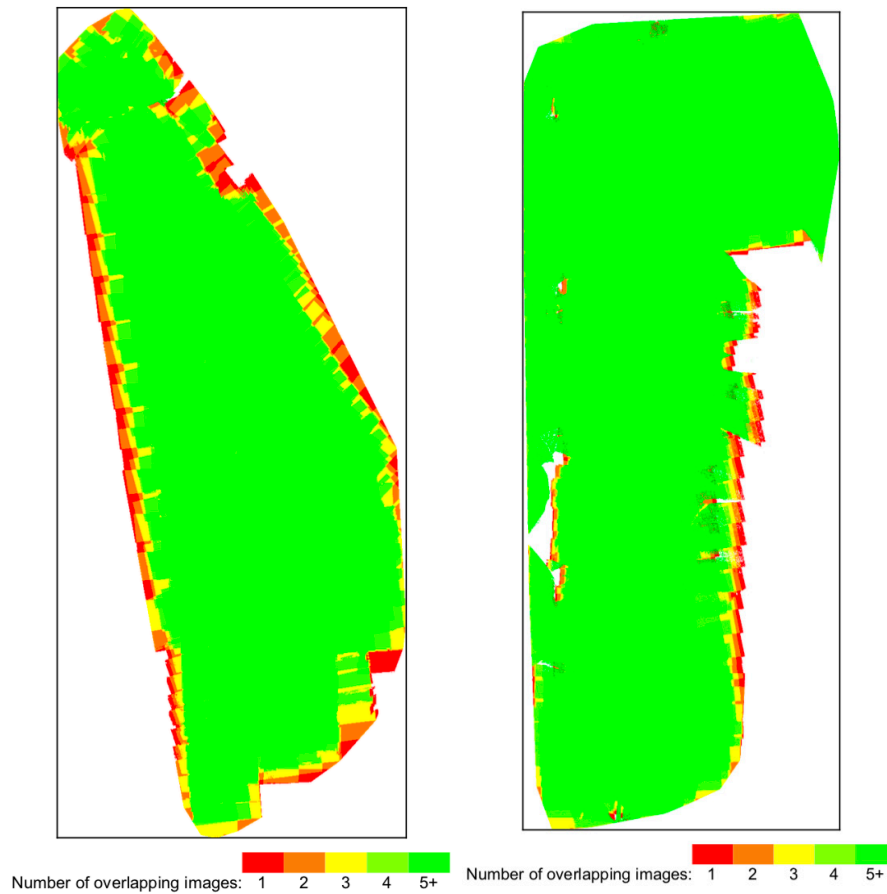


Figure 14. Image overlap results. Study site 1 (left), study site 2 (right). Red through yellow indicate poor overlap, green indicates high overlap from which good results were generated. Source: Pix4D quality reports.

To evaluate the accuracy and overall quality of the drone-generated orthomosaics, the differences between the initial and computed image positions were calculated, as shown in

Table 8. The difference between the initial and computed positions is the error. Large error values indicate that much stretching and skewing had to occur for the data to match. With high overlap and sub-centimeter ground sampling distances of 0.56 cm for study site 1 and 0.62 cm for study site 2, small error ranges were achieved between the initial and computed image positions for the study sites.

Table 8. Error assessment calculated as the difference between initial and computed positions.

	Bertrandt Study Site 1			German School Study Site 2		
	X	Y	Z	X	Y	Z
Mean absolute geolocation error (m)	-0.22	0.51	-0.07	-0.05	0.01	-0.10
Mean absolute camera position and orientation uncertainty (m)	0.046	0.042	0.113	0.547	0.322	0.640
Mean relative camera position and orientation uncertainty (m)	0.020	0.025	0.071	0.010	0.012	0.017
Relative geolocation error (cm)	±1.12	±0.56	±0.56	±0.62	±0.62	±0.62
Mean ground control point error (m)	.000002	.000003	.000001	0.0037	0.0013	-0.004
Mean root mean square (RMS) error	0.002 m			0.028 m		
Mean projection error (pixels)	0.165 pixels			0.210 pixels		

The mean absolute geolocation error for the Bertrandt study site was found to be -22 cm in the X direction, 51 cm in the Y direction, and -7 cm in the Z direction. The mean ground control point error was virtually zero. With such low error values and a GCP accuracy of 4 cm, the Bertrandt study site has achieved high quality results with centimeter (below one meter) level relative and absolute accuracy. The mean RMS error of 0.2 cm for study site 1 is very small,

indicating a good and consistent transformation accuracy. The orthomosaic generated for study site 1 is shown in Figure 15.



Figure 15. Bertrand parking lot orthomosaic; study site 1.

The mean absolute geolocation error for the German school study site was found to be -5 cm in X, 1 cm in Y, and -10 cm in Z. The mean ground control point error was 0.37 cm in X, 0.13 cm in Y, and -0.4 cm in Z. As described in Section 3.1.2, the GCPs in the German school study site were collected with a handheld GPS unit and achieved an average accuracy of 71 cm in XY direction and 91.5 cm in the Z direction. With low error values and sub-meter accurate GCPs, the German school study site 2 has achieved good quality results with centimeter level relative accuracy and absolute accuracy at or just below one meter. The mean RMS error of 2.8 cm for study site 2 is large, indicating issues and/or inconsistent transformation accuracy. Figure 16 shows the orthomosaic generated for study site 2. Inconsistencies and transformation issues can be seen along the edges of the orthomosaic.

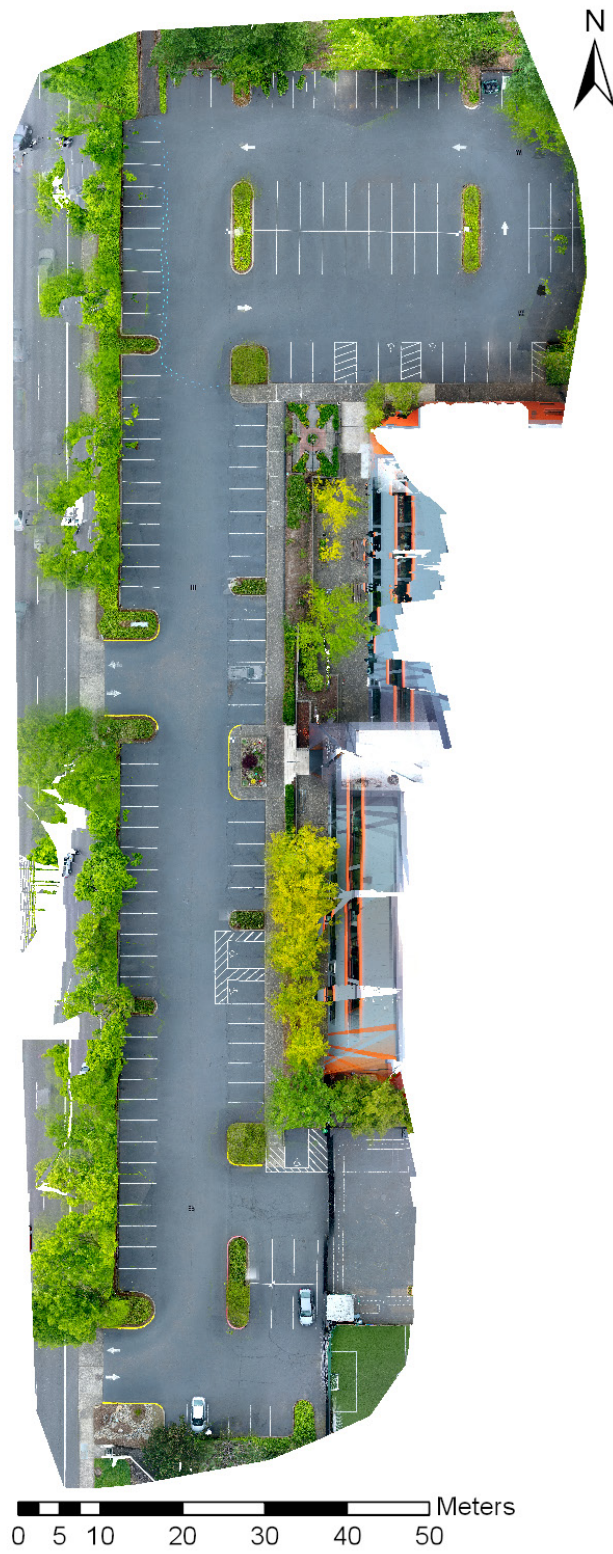


Figure 16. German school parking lot orthomosaic; study site 2

4.2. Manual Delineation Results

The Bertrandt study site and German School study site were successfully digitized by manual efforts. The required data structure for conversion to the NDS data format was followed. As the total area covered for both study sites was relatively small, the required time for manual digitizing was a few hours. As shown in Table 9, the total time for digitizing includes all feature classes such as roads, parking spots, parking areas, and green surfaces. The time to set up the data structure includes the editing of the attributes, running the tools to convert polygons to lines, and multipart to single part lines, running the tool to create the SQLite database, and exporting the feature classes as geopackages. Due to the large (1.07 GB) size of the Bertrandt study site orthomosaic, some of the digitizing time of the Bertrandt study site went to patiently waiting as the orthomosaic loaded.

Table 9. Time required for manual delineation.

	Bertrandt Study Site 1	German School Study Site 2
Total time for digitizing	4 hrs 43 min	1 hr 46 min
Time to set up data structure	25 min	20 min

Both study sites were successfully exported to geopackages as single line feature classes and sent to Andreas Pehlke at Bertrandt, Inc. to test NDS conversion. Figure 17 and 18 show the final data representations of study site 1 and 2 that were exported as line feature classes from ArcGIS Desktop. The BMD_LINES feature class marks the entry and exit border of the parking lot.

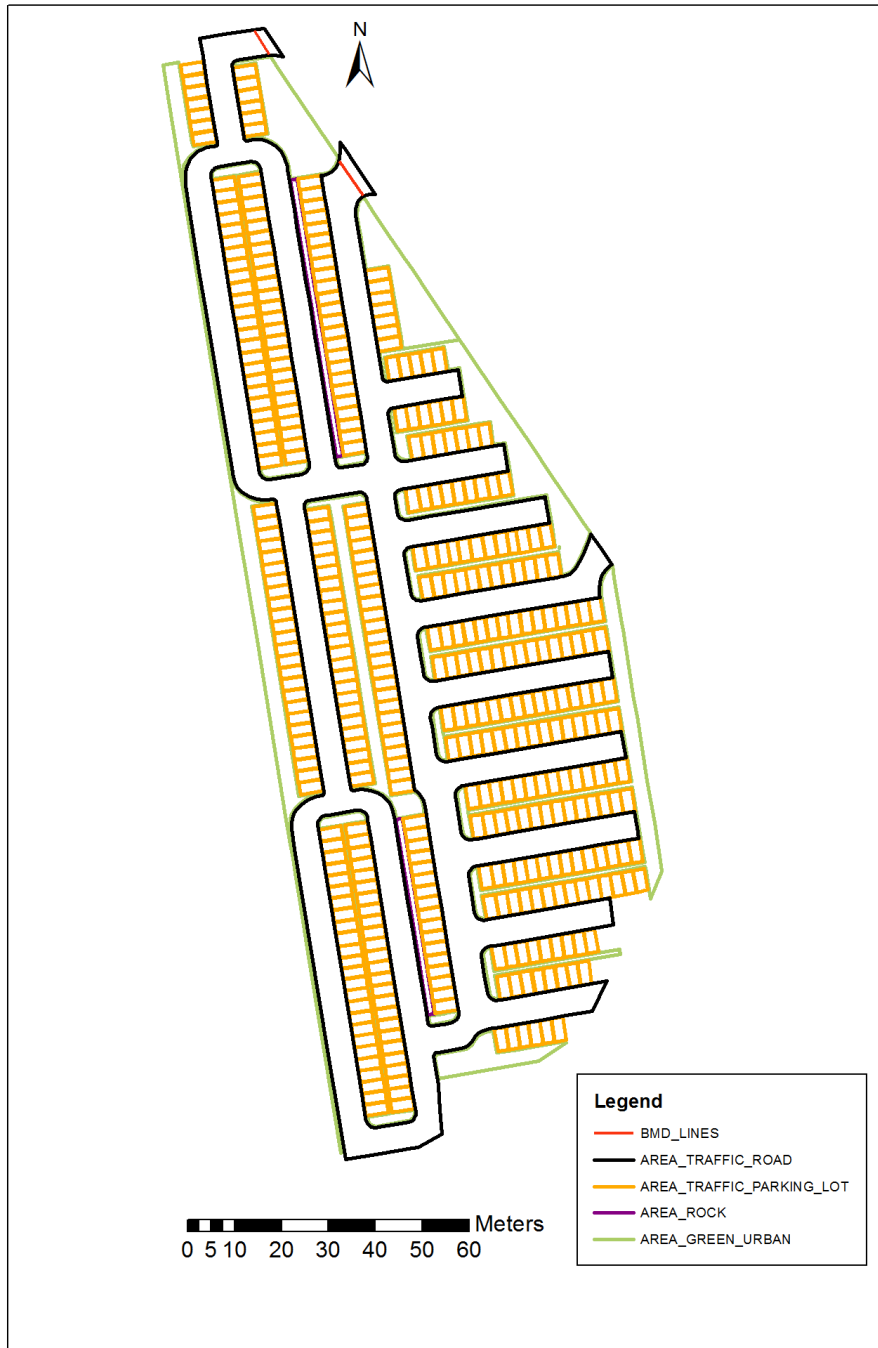


Figure 17. Manual delineation; final representation of study site 1.

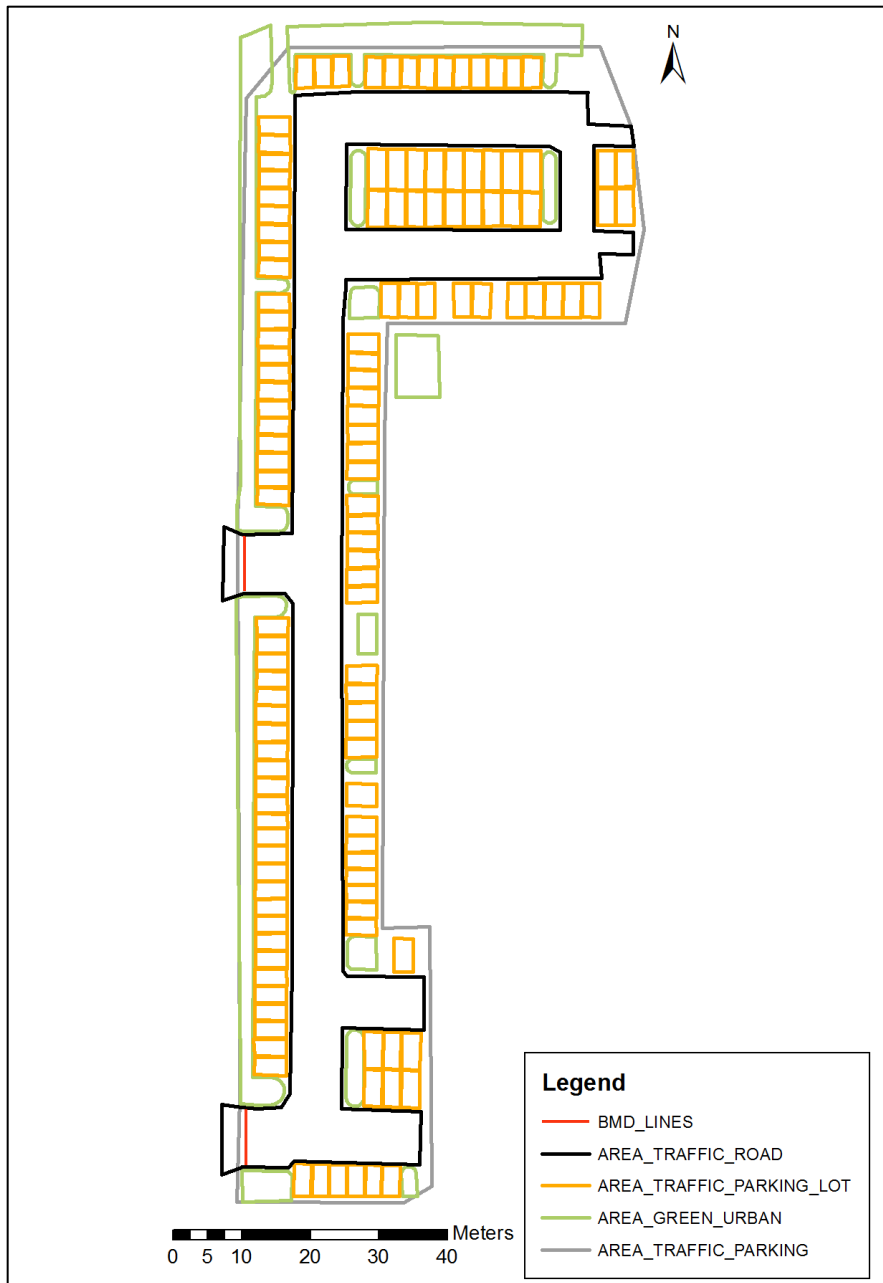


Figure 18. Manual delineation; final representation of study site 2.

4.3. Tool-based Extraction Results

The vector machine classification approach, in conjunction with Esri’s object-oriented feature extraction workflow and post-classification processing workflow, proved successful in extracting the specified features from the orthomosaic with little noise in the polygon feature classes created. For both study sites, the training samples entered in the Train Sample Manager wizard and used for supervised classification correctly grouped the specified objects into classes. From the orthomosaic to NDS-ready line feature classes, the total time for the Bertrandt study site was 9 hours and 33 minutes and for the German School study site 3 hours and 42 minutes. Compared to the manual delineation method, the manual input in the tool-based extraction was significantly less, with 10 minutes of manual input for the Bertrandt study site and 34 minutes for the German School study site. Table 10 shows in more detail the runtime for the tools and model components. The tools in Table 10 are grouped into components based on their processing purpose.

Table 10. Tool and model component runtime for tool-based extraction method.

Tool and Model component Runtime	Bertrandt Study Site 1	German School Study Site 2
Segment mean shift runtime	4 hrs 19 min	47 min
Vector support classification tools runtime (train support vector machine classifier, classify raster, reclassify)	3 hrs 11 min	1 hr 41 min
Post-processing tools runtime (boundary clean, region group, nibble, eliminate)	1 hr 49 min	35 min
Extension model runtime (tool run only time)	4 min	6 min
Autocomplete polygons (manual input)	N/A	24 min
Train sample manager (manual input)	10 min	10 min
Total time	9 hrs 33 min	3 hrs 42 min

The extraction process of features from the Bertrandt study site was successful and included vehicle, vegetation, parking area, and road extraction. The cobble stone pattern of the road was initially an issue as the road was divided into hundreds of small rectangle polygons. By use of the post-processing tools that removed insignificant pixel groups and polygons, the cobble stone pattern was, however, removed and the road was rendered correctly. The results of the main model run, orthomosaic to polygon feature class extraction, for the Bertrandt study site are shown in Figure 19. The results of the Bertrandt parking lot extension model run are shown in Figure 20. The result shown in Figure 20 is the final representation of the Bertrandt study site by tool-based extraction methods. Compared to the final representation by manual delineation (Figure 17), the results of tool-based extraction are more chaotic. The main reason for large differences between the processing methods for the Bertrandt study site is the fact that the vehicles were included in the tool-based extraction method but were ignored during manual delineation.

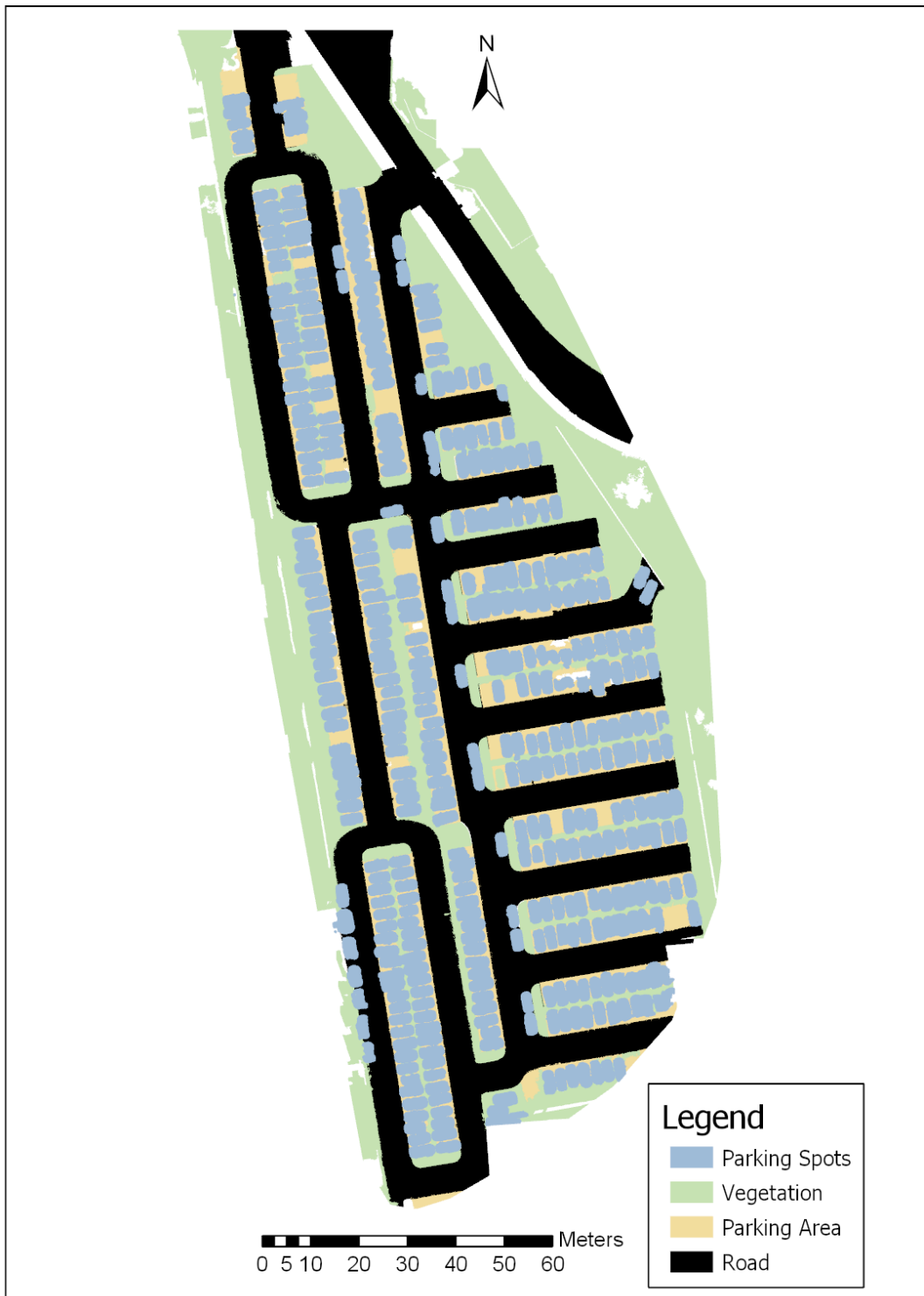


Figure 19. Main model result for the Bertrandt study site 1.



Figure 20. Bertrandt extension model result; final representation of study site 1.

The extraction processes of features from the German School study site were also successful and included parking spots, road, and vegetation. Figure 21 depicts the results of the main model run, orthomosaic to polygon feature classes, for the German school study site. The results of the German School extension model are shown in Figure 22. The extension model included the manual input to the “Autocomplete Polygons” tool to complete parking polygons out of the parking lines. With a manual input of 24 minutes, significantly less time was spent digitizing than by methods of manual delineation. Due to the lack of vehicles in the German school parking lot and the visibility of parking lines, the final representation shown in Figure 22 is significantly less chaotic than tool-based extraction results seen in study site 1.

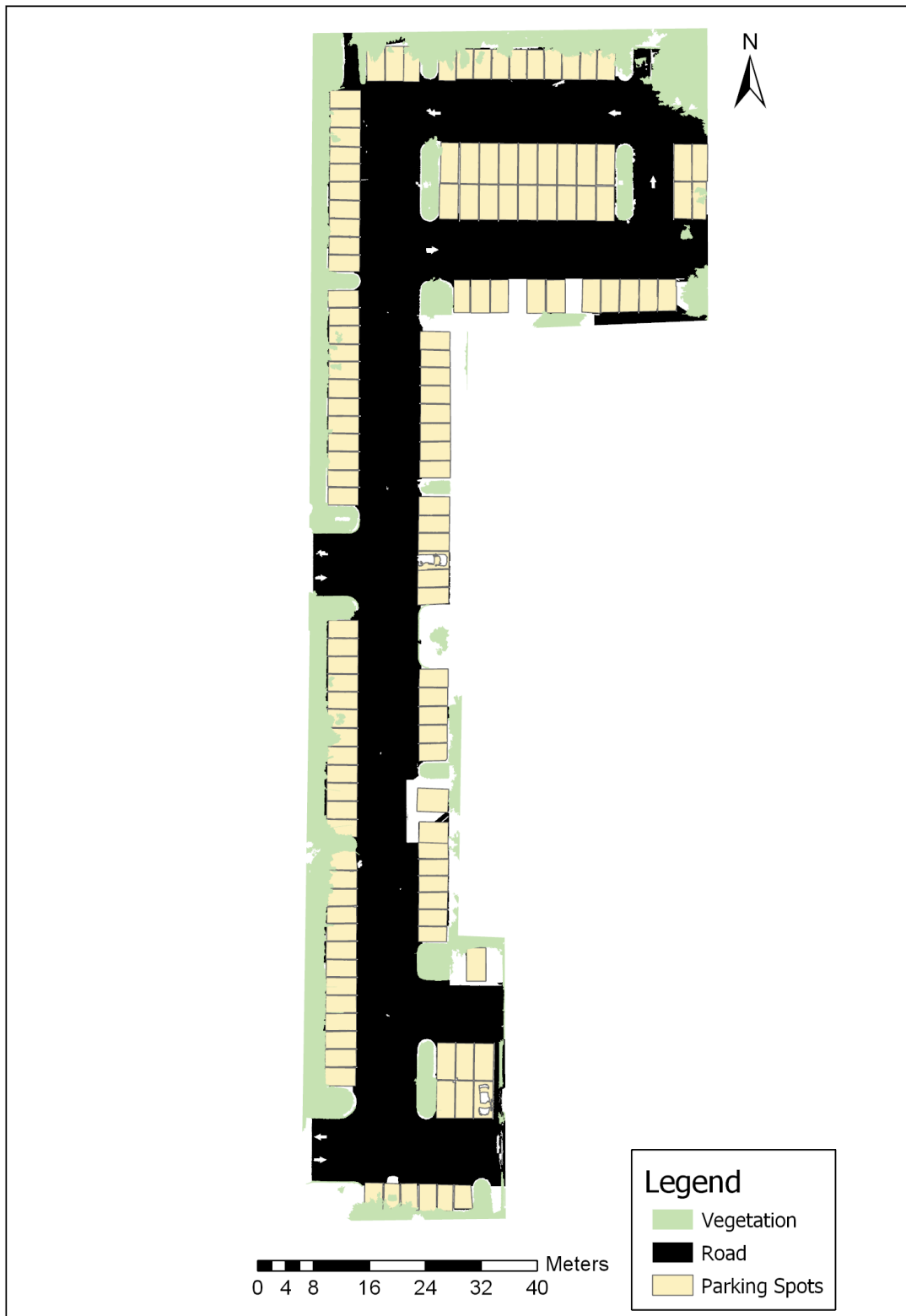


Figure 21. Main model result for the German School study site 2.

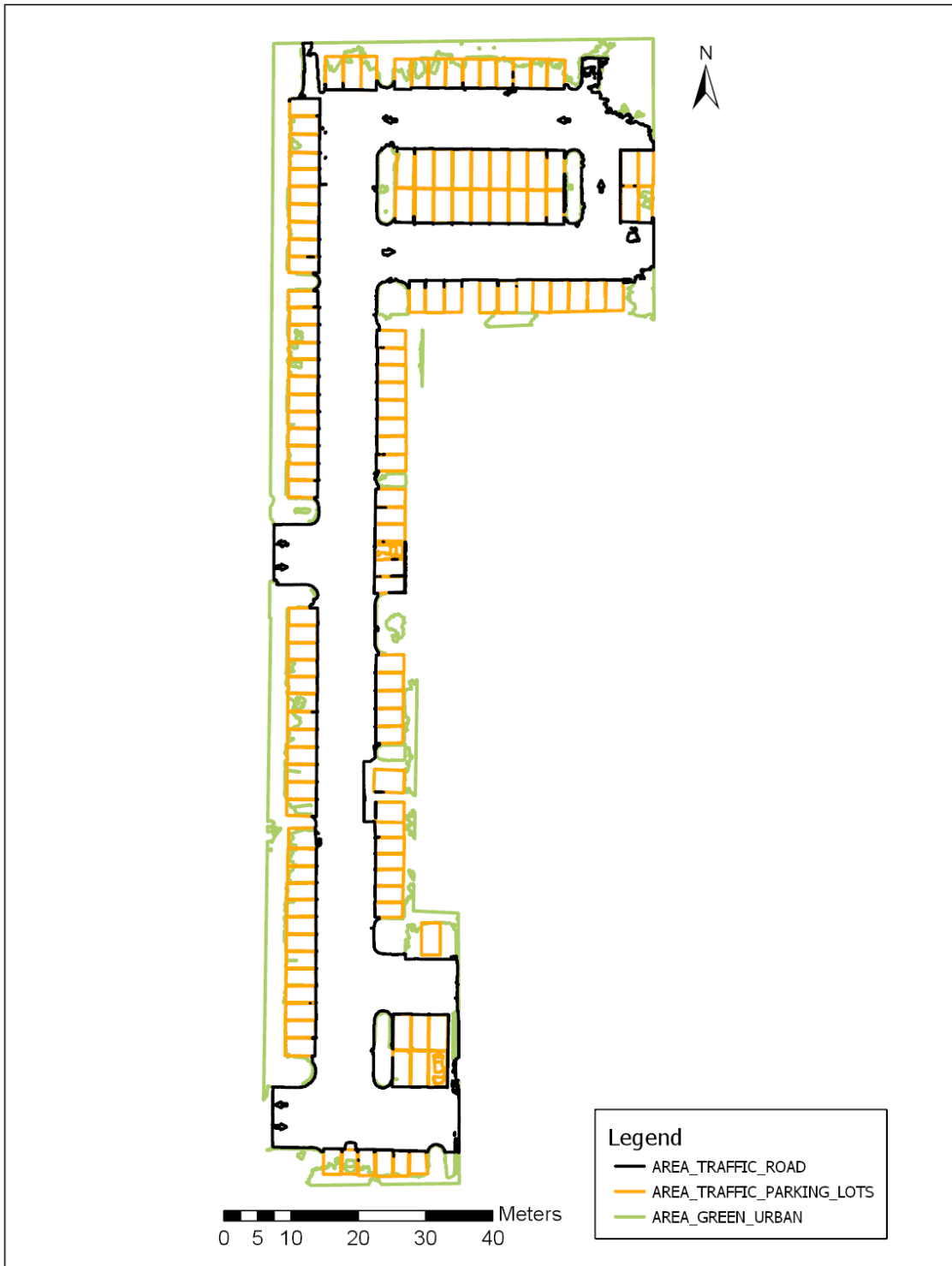


Figure 22. German School extension model result; final representation of study site 2.

4.4. NDS Conversion

The manual delineation results of the Bertrandt study site and German School study site were successfully converted to the NDS data format and the resulting datasets were successfully displayed in the NDS database Inspector. The tool-based extraction results of the study sites were successfully converted to the NDS data format but did not display in the NDS database Inspector.

In an e-mail thread with the author from June 23rd to July 16th, 2019, Bertrandt employee Andreas Pehlke explained that no objects were rendered for the tool-based extraction method in the NDS-database Inspector which is most likely due to the lack of order and direction in the vertices of the objects. Objects in the NDS format are only displayed if the vertices of the lines are in the correct order. The geometry type and attribute information were according to NDS format specifications and therefore ran through the conversion successfully. For the manual delineation method, the results were converted successfully but a few vertices had to be changed by relocating the vertex for correct display in the NDS-database Inspector.

The final NDS-formatted datasets from the output produced by the manual delineation method are shown in Figures 23 and 24 for study site 1 and study site 2, respectfully. The NDS formatted datasets are displayed in the NDS-database Inspector in Figures 23 and 24. In Figure 23, some discontinuity can be seen in the road feature class where vertices did not have the correct order or direction. The breaks in continuity can also be due to uncertainty in the specified coordinates of the vertices. With some manual adjustment in the NDS database, the coordinates of these vertices can be shifted.



Figure 23. Bertrand parking lot in NDS format. Parking spots and road are white, vegetation is green, exit and entry borders are purple, and rock area is black. Source: Andreas Pehlke, Bertrand, Inc.

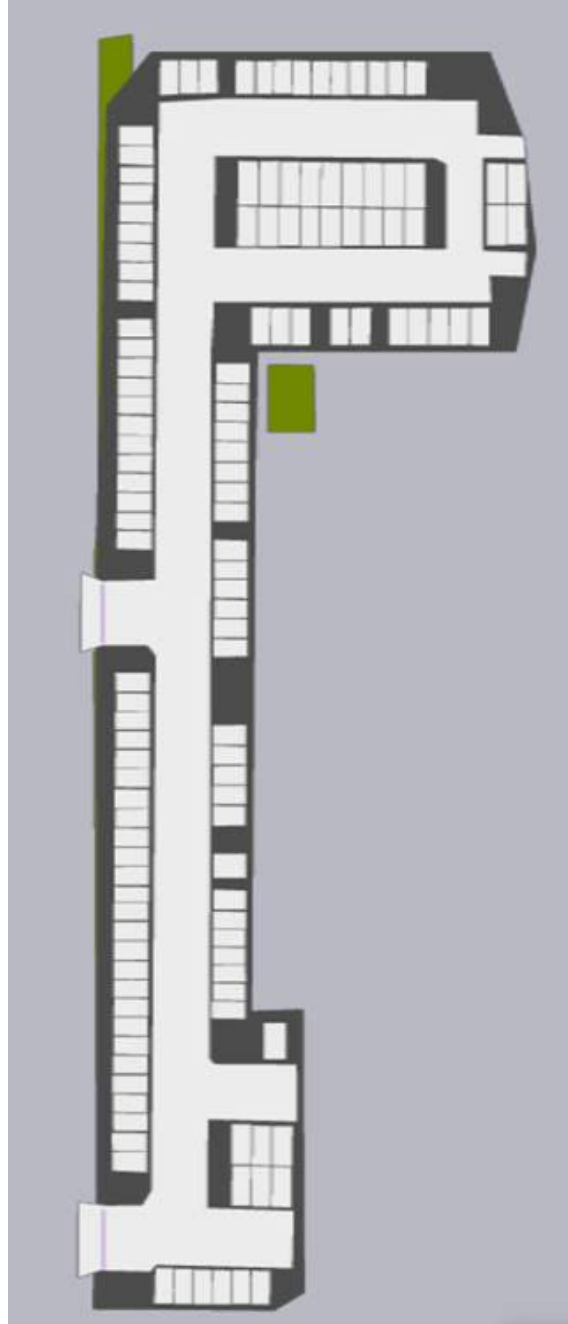


Figure 24. German School parking lot in NDS format. Parking spots and road are white, vegetation is green, exit and entry borders are purple, and the parking area boundary is black. Source: Andreas Pehlke, Bertrandt, Inc.

Chapter 5 Discussion and Conclusion

Although aerial drones have been used as a remote sensing method in fields such as agriculture and environmental studies, the drone-based remote sensing method and processing methods evaluated in this research study offer an initial investigation of an alternative approach to HD dataset development for use in autonomous vehicle navigation.

5.1. Current HD Data Standards and the Drone-generated HD Datasets

Described in Section 3.3, the HD data standards uncovered from communications with Here Inc., related literature research, and communication with Bertrandt Inc., specify that an HD dataset has an absolute accuracy at or below one meter and a relative accuracy below the absolute accuracy. The drone-generated orthomosaics showed that the accuracy for aerial imagery relies heavily on the accuracy of the ground control points (GCPs) and the ground sampling distance (GSD). According to the Pix4D website, relative accuracy is expected within one to three times the GSD, absolute accuracy is one to two times the GSD horizontally, and one to three times the GSD vertically, assuming the projects were reconstructed correctly. The Bertrandt study site had centimeter level absolute and relative accuracy errors with a GSD of 0.56 cm and a GCP accuracy of 4 cm. Assuming the Bertrandt study site was reconstructed correctly, the absolute and relative accuracy requirements were achieved at values far below one meter. The German School study site had absolute and relative accuracy errors in the 0-10 cm range with a GSD of 0.62 cm. The GCPs of the German School study site had an overall accuracy just below one meter. Assuming the German School study site was reconstructed correctly, the absolute and relative accuracy requirements were achieved with absolute accuracy values at approximately one meter.

The logistics of data collection by mapping-vehicles were compared to the data collection by the Phantom 4 drone, as shown in Table 11. Overall, this study showed that data collection by aerial drones can be a faster and more cost-efficient alternative method for data collection compared to mapping-vehicles.

Table 11. Data collection by mapping-vehicles vs. by aerial drone.

Data collection by mapping-vehicle	Data collection by aerial drone		
A stretch is driven 1-5 times for data collection.	The study sites were flown 2-3 times for data collection.		
Data volume is high from 3-5 GB per minute to multiple TB per hour.	Data volume was low at 1.5 GB to 2.5 GB per study site.		
Processing time, from data collection to HD dataset, is several days to weeks.	Total processing time	Study site 1	Study site 2
	With manual delineation	15.5 hrs	8.2 hrs
	With tool-based extraction	20 hrs	10 hrs
Mapping companies for hire can charge sums of \$5,000 per kilometer for their services.	The only additional cost in this study was purchase of a Pix4D license.		

The data volume obtained, time for data collection, and processing time by mapping-vehicles is significantly higher than the aerial imagery obtained and processed in this study. Important to remember, however, is that mapping-vehicles collect data with more than just one camera. A mapping-vehicle used in a study by Dolgov and Thrun 2009, depicts the use of a LiDAR sensor in addition to four different laser range finders (Dolgov and Thrun 2009). Combining the data output from all sensors and cameras during mapping results in high data volumes. The high data volumes, in turn, increase the processing time.

In this research study, a single-camera aerial drone was used to create high quality data. If drones can be used, it begs the question if high volume LiDAR sensing, in addition to the other sensors, is truly necessary to create a highly accurate map for use in autonomous vehicles. The company Waymo, which was formerly Google's self-driving car project, currently develops fully autonomous vehicles for shuttle and commercial services. These autonomous vehicles are equipped with three sensors; a 360-degree LiDAR sensor, a long-range sensor in the front, and a short-range sensor to monitor the car's perimeter (Randall 2019). If autonomous vehicles will be equipped with centimeter level sensors to navigate merely on their own, a high-quality map developed by means of aerial imagery may suffice.

5.2. Limitations and Challenges in Drone-based Data Collection

The allotted time for drone-based data collection at the Bertrandt study site in Germany was less than one week in January 2019. Within the week, weather challenges of rain and stormy winds limited data collection to three days. With flexible work hours at Bertrandt, Inc., the time of data collection was limited as well due to heavy people-traffic in the study site in the morning, at noon, and after 3:30 pm. With the limited possible flight time and weather uncertainty in January, the Bertrandt study site was flown in two parts during work hours. Unfortunately, parking at the Bertrandt company was limited and vehicles were present in the study site during data collection.

The orthomosaic generated for the Bertrandt study site experienced some challenges as well, as certain areas of the orthomosaic were distorted. Figure 25 illustrates the distortion of the northwest corner in the Bertrandt study site. The quality report generated for the Bertrandt parking lot shows that two blocks were generated for the calibrated images. This northwest region of the parking lot was separated into its own dataset block and thus extreme discontinuity

can be seen between the two blocks. The small northwest corner section was not tied well enough to the rest of the model. As a result, the northwest corner of the Bertrandt study site was not included in the processing.



Figure 25. Distortion in the northwest corner of the Bertrandt parking lot orthomosaic.

For the German School study site, no previously-surveyed benchmark points were available for use as GCPs, thus GCPs were measured with a GPS unit. Although a survey-grade

GPS unit would have been ideal for precise GCP marking, the accuracy of the GCPs in the German school study site were limited to the GPS unit available.

5.3. Proprietary Information

In addition to limitations and challenges faced during data collection, the lack of publicly available information on the subject surrounding autonomous driving posed another challenge. Literature and related work on subjects regarding the development of autonomous vehicles, high definition maps, HD map data structure, and current standards in the industry were very difficult to obtain or, for certain details, unobtainable. In particular, information regarding the data structure of HD maps and requirements for such maps was not publicly available. Fortunately, personal communication with members of participating companies provided some insight on the subject of HD maps and their structure. Yet even here, some information could not be shared due to the proprietary nature of the information.

Many automotive companies, their providers, and mapping companies are working towards self-driving cars and maps to support them. If HD maps are a key ingredient to make autonomous vehicles a reality, proprietary information on how to structure and create an HD map would not be publicly available as competing companies could use that information to their advantage. Even with a navigation data standard such as that being developed by the NDS consortium, the participating companies do not share their technological advancements with one another. Rather, the NDS format allows sharing of the end-products over various platforms.

5.4. The Feature Extraction Processes

The processing methods used in this research study included hands-on digitizing and object extraction by the use of various tools. The requirements of the final data structure were clear, and the processing methods were constructed accordingly. Manual delineation efforts

included the tracing of desired features in the orthomosaic and were a time-consuming process, however, the outputs were therefore very controlled. Feature extraction by use of various tools allows for significantly less manual input by the user. Successful combinations of tools can also result in an automated model run or script development to extract the desired features. The model workflows used in this research project were successful in extracting the desired features, however, tool parameters were tested by trial and error as no guidelines or related research could be found on tool-based extraction methods of parking lot features. In addition, the tools used did not allow directional input of the lines or polygons created. Line and vertex direction could not be predetermined for the tools, resulting in random line and vertex direction. As all data structure requirements were fulfilled in the tool-based extraction method, the line feature classes were converted to the NDS format. With random and non-readable vertex order, the resulting line feature classes could not be displayed in the NDS format.

The extraction of vehicles in the Bertrandt parking lot was difficult. Some vehicles were not parked correctly within the parking lines, other vehicles parked entirely on the road, and again other vehicles were parked so far in the parking space that the front of the vehicles overlapped into the vegetation extent (see Figure 26). In theory, extracting the vehicle as a polygon with a small buffer could render the approximate area of a parking spot, however, vehicles would have to be parked perfectly within the parking spot.

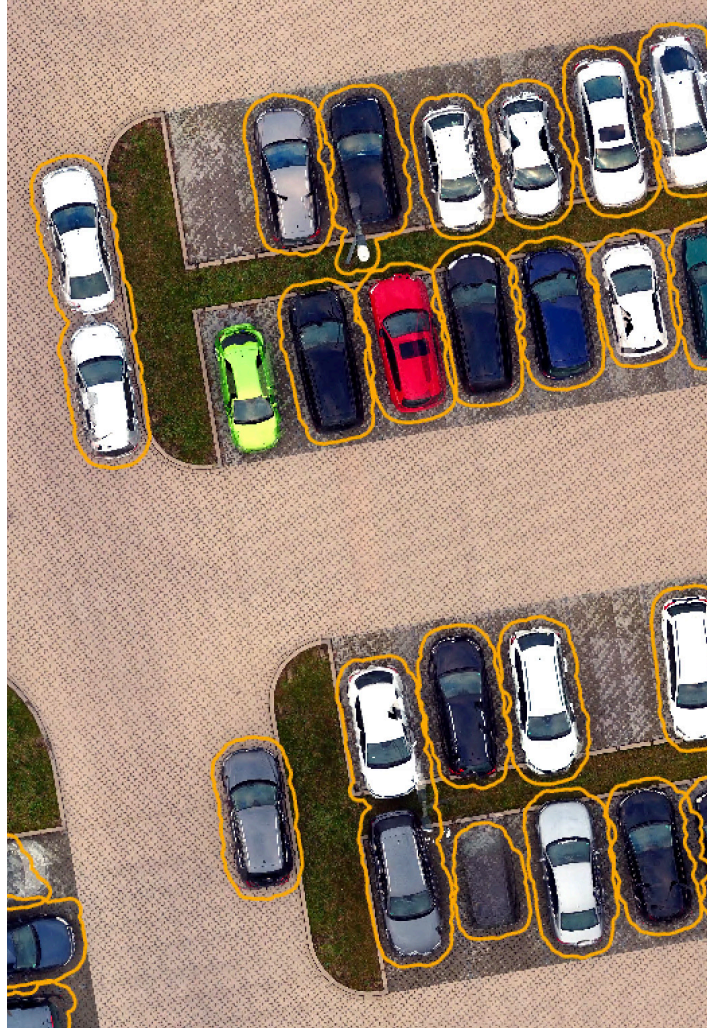


Figure 26. Illustration of parking spot challenge from vehicle extraction. Orange lines are the buffered parking spot lines.

The extraction of parking lines in the German School study site worked very well. The extracted parking lines rendered small polygons that matched the pattern of the parking spots. With some manual input, the parking spaces were created from the parking lines. Overall, the tool-based extraction results show that clearly marked parking spaces and empty parking lots are beneficial for tool-based feature extraction.

5.5. Future Research

The advantages of drone-based data collection are several, including the possibility of operating a number of drones at the same time. A large area, such as a company campus, could be flown by a number of drones within just minutes. Other advantages of drone-based data collection compared to traditional HD data collection methods include low-cost financial investment, small data volumes, and no fossil fuel combustion.

To further investigate the use of aerial drones as a means of data collection to develop HD maps, next steps may include the use of additional sensors or an upgraded aerial drone. As drone-based surveying methods are growing, miniature LiDAR sensors are available for installation on recreational drones. To gather point-cloud data similar to mapping-vehicles, LiDAR sensors could be added to the aerial drone. Upgrades could also include the use of a more accurate drone, such as a real-time kinematic (RTK) drone system. As implied by the name, RTK is a GPS correction technology technique in which location data is corrected in real-time while the survey drone captures the images (Rabkin 2018). Other advantages of new correction technologies, such as RTK or post-processing kinematic (PPK) techniques, includes the removal for need of ground control points (Rabkin 2018). The recreational Phantom 4 drone utilized in this research study could be replaced by its technologically advanced successor, the DJI Phantom 4 RTK. According to an accuracy study carried out by DroneDeploy, the Phantom 4 RTK delivers a relative horizontal accuracy of 1.2 cm and a linear measurement accuracy of 3.65 cm, without the use of GCPs (Willoughby 2019). Eliminating the need of GCPs would significantly decrease data collection time while maintaining high accuracy standards. At a price of \$6,500, the Phantom 4 RTK drone would continue to be a cost-efficient alternative to sensor-equipped mapping-vehicles.

Future development may also include 3D aerial drone flights instead of, or in addition to, 2D flights. As described in Section 3.1, tree canopy clearance can be difficult when capturing 2D imagery. Flight routes must be planned to be flown at an altitude that allows for tree canopy clearance to avoid collisions. Unfortunately, the tree canopy often covers roads and other objects that are important for extraction. Mapping on a 3D instead of 2D plane would allow the drone to fly below the tree canopy line. In cases where roads are bordered by rows of trees that cover the road from above, flying the drone on a 3D plane would allow the road to be followed and mapped below the trees. Adding 3D flights would also allow the mapping of important features such as bridges or powerlines that do not appear well in a 2D space. Knowing the existence of bridges and powerlines and what heights they are would be extremely important for vehicles above average heights, such as semi-trailer trucks. Another advantage of 3D flight includes the generation of dense point clouds, similar to points clouds created by LiDAR sensors. From the point clouds, additional information could be calculated such as traffic-light heights or bridge heights.

Other future research could include the development of a tool or application that could specify the direction of vertices in automatically extracted vector feature classes. Once the order and direction of vertices in the lines can be determined, tool-based extracted objects from aerial images could be displayed in the NDS format. As the method of manual delineation has clearly defined and known values, this research study could be expanded to include a confusion matrix that compares the results from the different methods. The confusion matrix would evaluate the performance of the classification models. For example, the manual delineation method and tool-based extraction method could be compared by dropping 1000 points on top of each dataset and then comparing the extracted land uses found.

5.6. Final Conclusions

The use of drone-based remote sensing techniques to develop high quality datasets has proven effective and accurate. With use of ground control points or other GPS correction techniques, a low-cost drone could serve as an alternative mapping-method to current leading mapping-techniques for the development of HD maps for autonomous vehicles.

Manual delineation was successful in extracting the desired features from the drone-generated orthomosaics. Although manual delineation is a time-consuming process, the direction of lines and vertices drawn can be controlled and is thus still the best-suited option for dataset conversion to the NDS format. The tool-based extraction method applied a supervised classification process by use of training samples, in addition to post-processing methods, and proved effective in extracting objects from high resolution orthomosaics. The required data structure for conversion to the NDS format was followed successfully and all datasets were converted. Unfortunately, vertex direction could not be controlled in the tool-based extraction technique and thus the resulting datasets could not be displayed in the NDS database inspector. As the use of aerial drones and the data volume of imagery increases, the need for an automated tool method to derive certain land covers increases. With further modifications to the tool-based extraction method, it would show superior results to manual delineation.

Overall, this research shows that aerial drones are capable of producing high quality imagery that can be used for HD map development, all in a time-efficient, cost-efficient, and environmentally friendly manner.

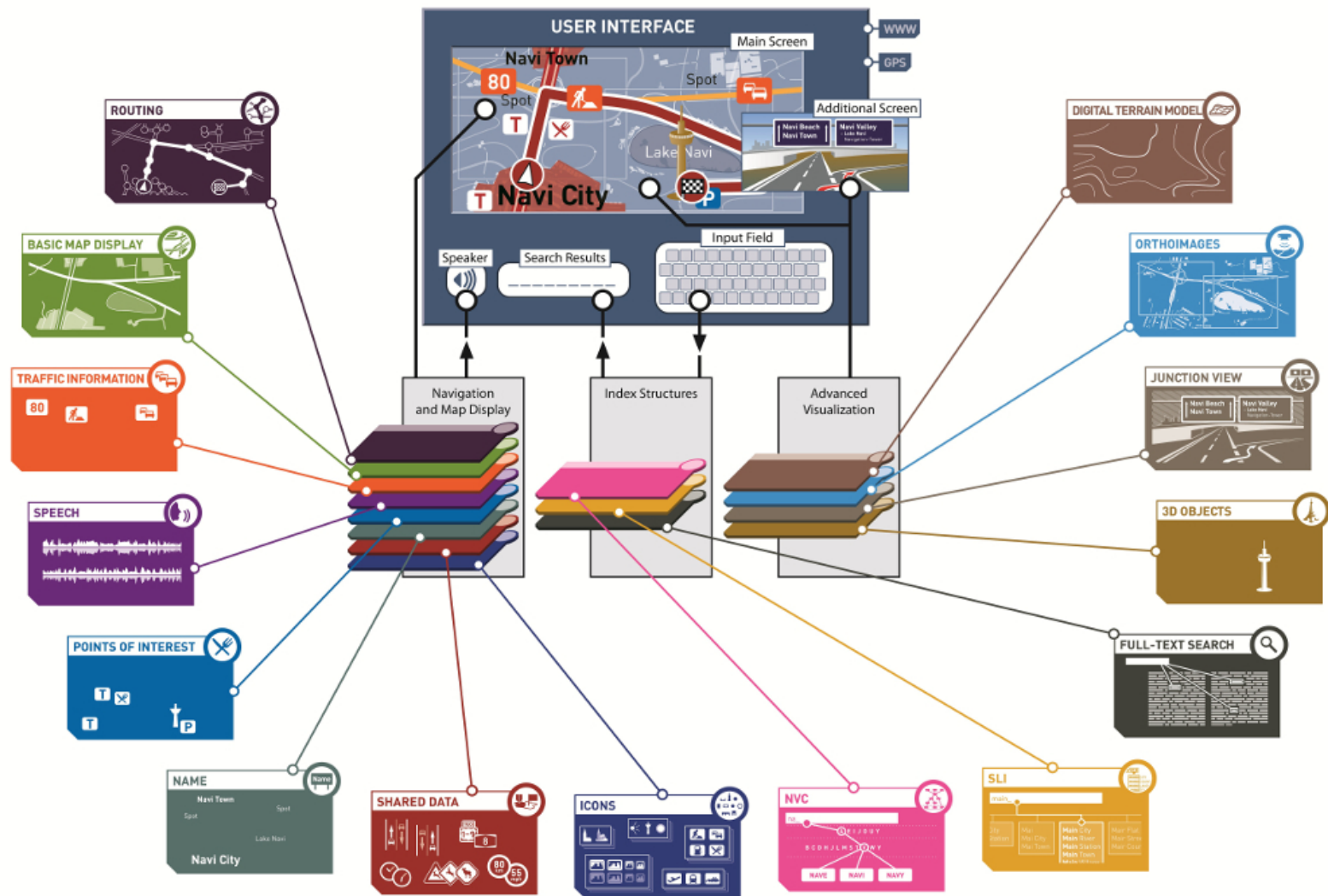
References

- Automotive World. 2018. "HD maps--the key to autonomous driving success?" *Automotive World*, October 3, 2018. <https://www.automotiveworld.com/articles/hd-maps-the-key-to-autonomous-driving-success/>.
- Bonetti, Pino. 2016. "HERE introduces HD Live Map to show the path to highly automated driving HD map" *Disqus*, January 5, 2016. <https://360.here.com/2016/01/05/here-introduces-hd-live-map-to-show-the-path-to-highly-automated-driving/>.
- Centers for Disease Control and Prevention. 2017. "Global Road Safety." Last modified June 7, 2017. <https://www.cdc.gov/motorvehiclesafety/global/index.html>.
- Chellapilla, Kumar. 2018. "Rethinking Maps for Self-Driving." *The Medium*, October 15, 2018. <https://medium.com/@LyftLevel5/https-medium-com-lyftlevel5-rethinking-maps-for-self-driving-a147c24758d6>.
- Chen, Anning, Arvind Ramanandan, and Jay A. Farrell. 2010. "High-precision lane-level road map building for vehicle navigation." Paper presented at the *IEEE/ION Position Location and Navigation Symposium (PLANS)*, Indian Wells, CA, May 4-6, 2010, 1035-1042. <http://social.ion.org/wp-content/uploads/2013/06/Presentation.pdf>.
- Dokic, Jadranka, Beate Müller, and Gereon Meyer. 2015. "European roadmap smart systems for automated driving." *European Technology Platform on Smart Systems Integration*, April 1, 2015. <http://www.a3ps.at/site/sites/default/files/newsletter/2015/no08/EPOSS.pdf>.
- Esri. 2019. "Multipart To Singlepart." <http://desktop.arcgis.com/en/arcmap/latest/tools/data-management-toolbox/multipart-to-singlepart.html>
- Hyatt, Kyle. 2018. "Here's why people still crash with driver assistance systems." *Road Show*, June 14, 2018. <https://www.cnet.com/roadshow/news/heres-why-people-still-crash-with-driver-assistance-systems/>.
- Here Technologies. 2018. "HD Live Map Data Specification." <https://developer.here.com/olp/documentation/hd-live-map/topics/hdlm2-logical-road.html>.
- Klemas, Victor V. 2015. "Coastal and environmental remote sensing from unmanned aerial vehicles: An overview." *Journal of Coastal Research* 31 (5): 1260-1267. doi: 10.2112/JCOASTRES-D-15-00005.1.
- Kent, Leo. 2015. "HERE introduces HD maps for highly automated vehicle testing." *Disqus*, July 20, 2015. <https://360.here.com/2015/07/20/here-introduces-hd-maps-for-highly-automated-vehicle-testing/>.
- Kummerle, Rainer, Dirk Hahnel, Dmitri Dolgov, Sebastian Thrun, and Wolfram Burgard. 2009. "Autonomous driving in a multi-level parking structure." In *2009 IEEE International*

- Conference on Robotics and Automation, Kobe, Japan, May 12-17, 2009*, 3395-3400. doi: 10.1109/ROBOT.2009.5152365.
- Litman, Todd. 2017. "Autonomous vehicle implementation predictions: Implications for Transport Planning." *Victoria Transport Policy Institute*, March 18, 2019. <https://www.vtpi.org/avip.pdf>.
- Laliberte, Andrea S., Jeffrey E. Herrick, Albert Rango, and Craig Winters. 2010. "Acquisition, orthorectification, and object-based classification of unmanned aerial vehicle (UAV) imagery for rangeland monitoring." *Photogrammetric Engineering & Remote Sensing* 76, (6): 661-672. doi: 10.14358/PERS.76.6.661.
- Massow, Kay, B. Kwella, N. Pfeifer, F. Häusler, Jens Pontow, Ilja Radusch, Jochen Hipp, Frank Dölitzscher, and Martin Hauéis. 2016. "Deriving HD maps for highly automated driving from vehicular probe data." In *2016 IEEE 19th International Conference on Intelligent Transportation Systems (ITSC), Rio de Janeiro, Brazil, November 1-4, 2016*, 1745-1752. doi: 10.1109/ITSC.2016.7795794.
- National Highway Traffic Safety Administration (NHTSA). 2018. "Traffic Safety Facts." Last modified April, 2018. <https://crashstats.nhtsa.dot.gov/Api/Public/ViewPublication/812517>
- Navigation data standard. 2019. "What is NDS?" <https://nds-association.org>
- O'Neill-Dunne, Jariath. 2015. "Image boost: drones produce sharper images for mapping." *Roads & Bridges* 53 (9). <https://trid.trb.org/view/1372835>.
- Pix4D. 2019. "What is accuracy in an aerial mapping project?" Last modified April 25, 2019. <https://www.pix4d.com/blog/accuracy-aerial-mapping>.
- Putch, Andy. 2018. "Linear Measurement Accuracy of DJI Drone Platforms and Photogrammetry." *DroneDeploy*, February 27, 2018. <http://imageryelevated.com/linear-measurement-accuracy-of-dji-drone-platforms-and-photogrammetry/>.
- Rabkin, Barry. 2018. "GCPs v. PPK/RTK: Which is Best to Receive Fast and Accurate Data?" *Identified Technologies*, July 12, 2018. <https://www.identifiedtech.com/blog/drone-technology/gcps-ppk-rtk-best-receive-fast-accurate-data/>.
- Randall, Tom. 2019. "Waymo starts selling sensors to lower cost of self-driving cars." *Bloomberg*, March 6, 2019. <https://www.bloomberg.com/news/articles/2019-03-06/waymo-starts-selling-sensors-to-lower-cost-of-self-driving-cars>.
- Seif, Heiko G., and Xiaolong Hu. 2016. "Autonomous driving in the iCity—HD maps as a key challenge of the automotive industry." *Engineering* 2 (2): 159-162. doi: 10.1016/J.ENG.2016.02.010.

- Synced. 2018. "The Golden Age of HD Mapping for Autonomous Driving" *The Medium*, August 11, 2018. <https://medium.com/syncedreview/the-golden-age-of-hd-mapping-for-autonomous-driving-b2a2ec4c11d>.
- TomTom. 2015 "TomTom delivers HAD Map for all highways in Germany." Last modified September 14, 2015. <https://corporate.tomtom.com/news-releases/news-release-details/tomtom-delivers-had-map-all-highways-germany?ReleaseID=931328>
- TomTom. 2017 "HD Map; Highly Accurate Border-To-Border Model of The Road." <http://download.tomtom.com/open/banners/HD-Map-Product-Info-Sheet-improved-1.pdf>.
- TomTom. 2018. "TomTom HD Map with RoadDNA; High definition Map with Sensor-Agnostic Localization." <https://www.tomtom.com/automotive/automotive-solutions/automated-driving/hd-map-roaddna/>.
- Tzotsos, Angelos, and Demetre Argialas. 2008. "Support vector machine classification for object-based image analysis." In *Object-Based Image Analysis*, 663-677. Springer, Berlin, Heidelberg.
- Van Brummelen, Jessica, Marie O'Brien, Dominique Gruyer, and Homayoun Najjaran. 2018. "Autonomous vehicle perception: The technology of today and tomorrow." *Transportation research part C: emerging technologies* 89 (April): 384-406. doi: 10.1016/j.trc.2018.02.012.
- Vardhan, Harsha. 2017. "HD Maps: New age maps powering autonomous vehicles." *Geospatial World*, September 22, 2017. <https://www.geospatialworld.net/article/hd-maps-autonomous-vehicles/>.
- Willoughby, James. 2019. "DJI Phantom 4 RTK: Survey-grade accuracy confirmed!" *Heliguy*, January 31, 2019. <https://www.heliguy.com/blog/2019/01/31/dji-phantom-4-rtk-accuracy-confirmed/>.
- Winner, Hermann, Stephan Hakuli, and Gabriele Wolf. 2009. "Digitale Karten im Navigation Data Standard Format." In *Handbuch Fahrerassistenzsysteme: Grundlagen, Komponenten und Systeme für aktive Sicherheit und Komfort*, 514-518. Springer Vieweg.
- Xiang, Haitao, and Lei Tian. 2011. "Development of a low-cost agricultural remote sensing system based on an autonomous unmanned aerial vehicle (UAV)." *Biosystems engineering* 108 (2): 174-190. doi: 10.1016/j.biosystemseng.2010.11.010.

Appendix A: Enlarged Version of the NDS Building Blocks



Appendix B: Questions and Answers from HERE Technologies

The following questions were sent to contacts at HERE technologies and were answered by Timm Kayser, the Sr Automotive Product Manager- HAD. The questions and answers are unaltered from the E-mail response.

1. What is the geolocation accuracy in a HD map?

We do have an accuracy of <1m absolute overall and for some features <50cm. Important to mention is: The absolute accuracy is always higher than the relative accuracy. Here is, why that matters: If you are an autonomous vehicle, you want to know, where in the lane you are. That boils down to your relative position between lane markings. Those two lane markings have a higher relative accuracy, as if you would try to compare an absolute lane marking position in Berlin, Germany to an absolute lane marking position in Munich. Thus, absolute accuracy is just “one side of the coin”.

2. How often has one track to be driven to create a HD map? Is one track enough for high accuracy?

HERE True vehicles drive on an “as needed” basis. Re-drives of known routes only happen if there is an indicator for change (e.g. construction zone information). With that strategy we make sure, not to re-drive on routes that haven’t changed. The strategy behind our fleet management is pretty complex. But this is the basic underlying principle. HERE True vehicles do drive a map link only once and collect high frequency and highly accurate information (e.g. lidar point clouds) which are processed offline later on.

3. During data collection, how fast can a mapping car be driven?

The speed is fairly low and (to my knowledge) have a maximum of 80km/h in speed. Here is why: The lidar sensor is a rotating sensor pod that does a 360°-ground 10 times per second. That means, that we have 10 “snapshots” per seconds. If you stand still, the lidar points at the always same locations. If you start to move, you barely hit the same point again. The faster you move, the more “sparse” the 3D point cloud gets. “sparse” means, that the distance between collected lidar points raises the faster you drive. The “speed for data collection” now is a tradeoff between “density of point cloud” and “speed of mapping”.

4. For a stretch of 1 km, how much data volume will be required for HD maps?

The answer highly depends on what you want to achieve. If you think about HERE True, we do talk about 60-80Mbyte/second of raw data from lidar + 80Mpixel imagery being collected at 20Hz. Quite a lot of data. HERE HAD uses HERE True to map new roads initially, but uses OEM fleet vehicle data to maintain the initially created map. If we do talk about sensor data amounts from OEM vehicles, we do talk about 80-100Kbyte/km. These “OEM sensor data” are segmented and highly aggregated/compressed data, whereas the HERE True collection targets raw sensor data collection. As you might see, the effective data amount for mapping ranges from “multiple Gbyte per KM” down to “couple dozen Kbyte/km”. It depends on what you want to achieve.

5. How much time (also processing time) is needed from data collection until a HD map is completed and ready to be used for an autonomous vehicle?

The answer again heavily depends on what you want to achieve. If you map a new road initially with HERE True raw sensor data, you need to perform heavy lifting to get the essential content out of lidar point clouds, raw imagery and high-frequency pose points. It takes quite a while to process all the data, align the content to the existing map, connect the new information (e.g. a lane marking geometry to the existing map content), etc. ... In some cases, ambiguity cannot be resolved by algorithms (e.g. a complex intersection in urban areas). In those cases, we need to ask your colleagues in QA (Quality Assurance) to manually inspect the generated map content before we release it to customers. ... Map making isn't easy. ;) And it might require days to generate a map from scratch. ... However, there is a good message here: Once we have done an initial mapping, in HAD we target a 24hrs-turnaround-cycle. What does that mean? It means, that if we consume already aggregated segmented content from OEM vehicles (the couple dozen Kbytes mentioned in Question 4), we are able to incorporate changes within 24hrs. ... That operation can of course only be performed, if we do get enough data density per geographic region, as we do not blindly trust a data submission from one OEM vehicle, but wait until we have enough confidence that the observations are actually correct. Consequently, 24hrs-freshness can only be achieved, if we have sufficient inflow. ... Long story short: time-span is: Couple Days (even weeks) down to 24hrs.

6. Does a HD map of a parking lot exist? How is the structure of such a map? Is there one track to each single parking space?

HAD is currently focused on Limited Access Road network coverage. "Limited Access" roads are roads, where you have physical dividers between roads. Based on our collaborations with multiple OEMs, we see autonomous driving vehicles on those road types first before entering urban scenarios. Furthermore, "urban" scenarios for fully autonomous driving is what we see in the near/mid future and work on those aspects. "Parking" is not directly covered by HAD for now. However, HERE was working on a Parking Geometry product but that one has been de-prioritized lately to focus on the use cases mentioned above. ... But the basic strategy for HD Mapping is to capture physical objects (e.g. parking spot markings) you can actually touch (with your fingers). That means, that if we enter parking scenarios, we will likely map visual markings, walls, boardwalks, etc. and no "meta-objects" such as: virtual stopping locations, etc. Hope that helps.

Appendix C: Bertrandt Parking Lot; Pix4D Quality Report

Quality Report



Generated with Pix4Dmapper Pro version 3.0.18

Important Click on the different icons for:

- Help to analyze the results in the Quality Report
- Additional information about the sections

Click [here](#) for additional tips to analyze the Quality Report

Summary

Project	bertrandtparkplatz_ss1
Processed	2019-05-28 18:55:39
Camera Model Name(s)	FC330_3_6_4000x3000 (RGB)
Average Ground Sampling Distance (GSD)	0.56 cm / 0.22 in
Area Covered	0.0184 km ² / 1.8387 ha / 0.0071 sq. mi. / 4.5459 acres
Time for Initial Processing (without report)	01h:06m:11s

Quality Check

Images	median of 33187 keypoints per image	
Dataset	394 out of 413 images calibrated (95%), all images enabled, 2 blocks	
Camera Optimization	1.64% relative difference between initial and optimized internal camera parameters	
Matching	median of 12795.6 matches per calibrated image	
Georeferencing	yes, 3 GCPs (3 3D), mean RMS error = 0.002 m	

Preview

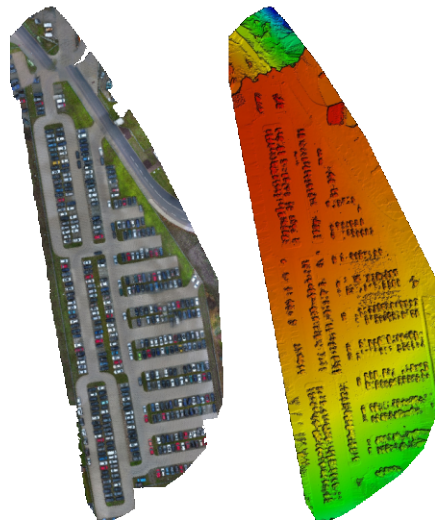


Figure 1: Orthomosaic and the corresponding sparse Digital Surface Model (DSM) before densification.

Calibration Details

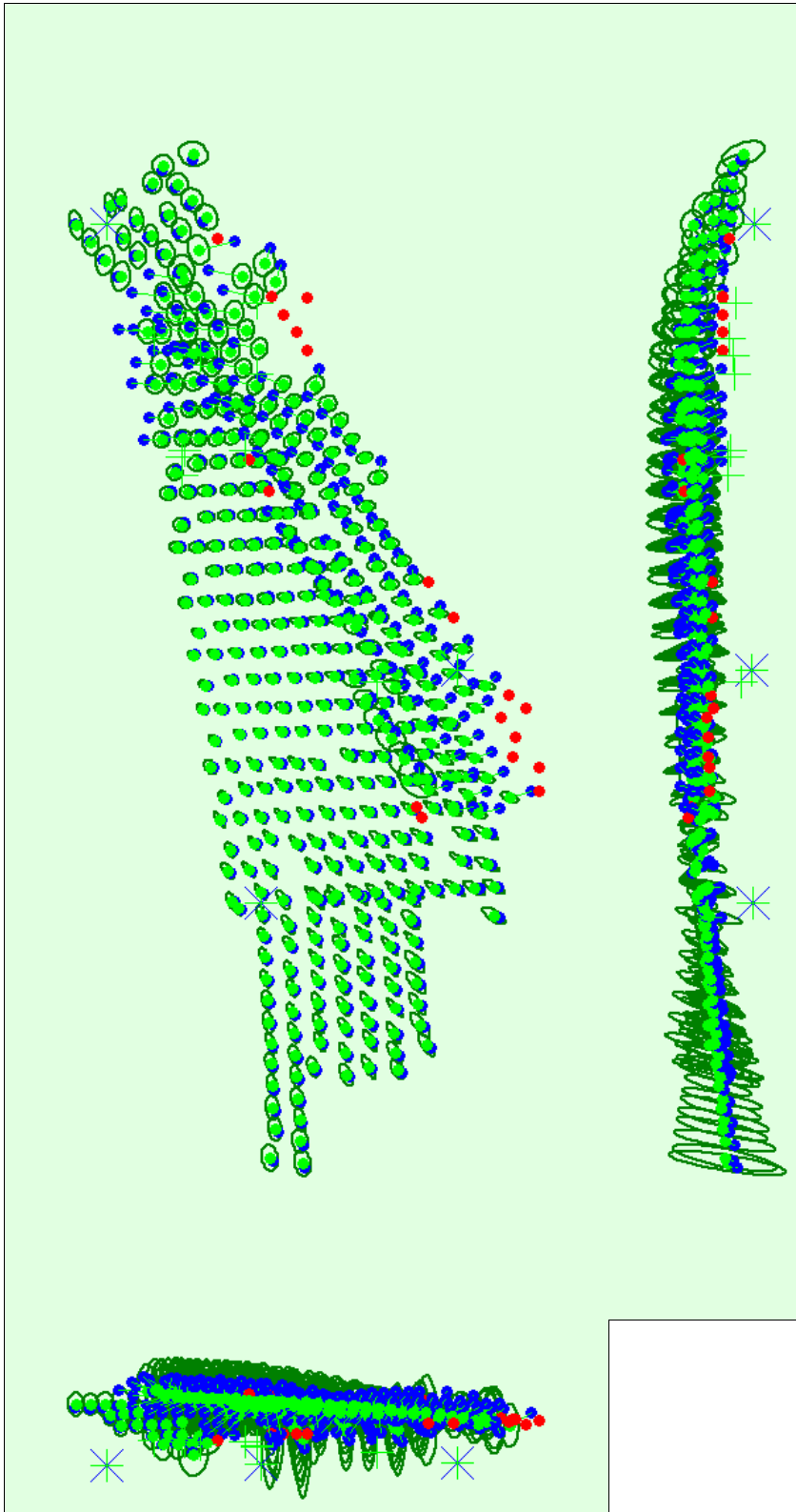
Number of Calibrated Images	394 out of 413
Number of Geolocated Images	413 out of 413

Initial Image Positions



Figure 2: Top view of the initial image position. The green line follows the position of the images in time starting from the large blue dot.

Computed Image/GCPs/Manual Tie Points Positions



Uncertainty ellipses 50x magnified

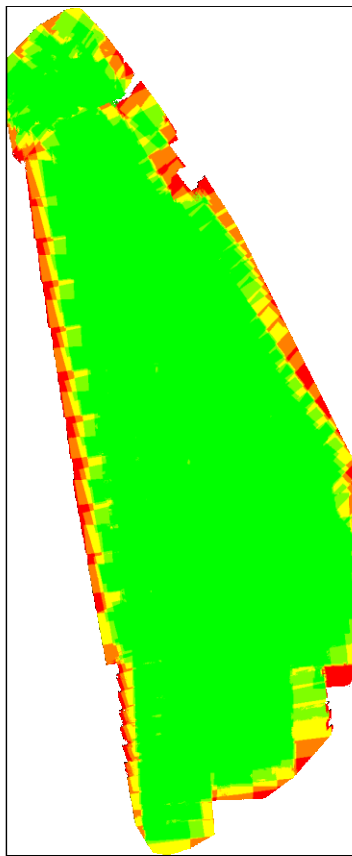
Figure 3: Offset between initial (blue dots) and computed (green dots) image positions as well as the offset between the GCPs initial positions (blue crosses) and their computed positions (green crosses) in the top-view (XY plane), front-view (XZ plane), and side-view (YZ plane). Red dots indicate disabled or uncalibrated images. Dark green ellipses indicate the absolute position uncertainty of the bundle block adjustment result.

🔍 Absolute camera position and orientation uncertainties



	X [m]	Y [m]	Z [m]	Omega [degree]	Phi [degree]	Kappa [degree]
Mean	0.046	0.042	0.113	0.157	0.136	0.037
Sigma	0.009	0.015	0.054	0.075	0.052	0.028

🔍 Overlap



Number of overlapping images: 1 2 3 4 5+

Figure 4: Number of overlapping images computed for each pixel of the orthomosaic. Red and yellow areas indicate low overlap for which poor results may be generated. Green areas indicate an overlap of over 5 images for every pixel. Good quality results will be generated as long as the number of keypoint matches is also sufficient for these areas (see Figure 5 for keypoint matches).

Bundle Block Adjustment Details



Number of 2D Keypoint Observations for Bundle Block Adjustment	4987301
--	---------

Number of 3D Points for Bundle Block Adjustment	1863851
Mean Reprojection Error [pixels]	0.165

Internal Camera Parameters

FC330_3.6_4000x3000 (RGB). Sensor Dimensions: 6.317 [mm] x 4.738 [mm]

EXIF ID: FC330_3.6_4000x3000

	Focal Length	Principal Point x	Principal Point y	R1	R2	R3	T1	T2
Initial Values	2285.722 [pixel] 3.610 [mm]	2000.006 [pixel] 3.159 [mm]	1500.003 [pixel] 2.369 [mm]	-0.001	-0.002	0.000	-0.001	-0.001
Optimized Values	2323.287 [pixel] 3.669 [mm]	2005.024 [pixel] 3.167 [mm]	1516.178 [pixel] 2.395 [mm]	0.006	-0.010	0.004	-0.000	0.000
Uncertainties (Sigma)	7.621 [pixel] 0.012 [mm]	0.863 [pixel] 0.001 [mm]	0.632 [pixel] 0.001 [mm]	0.001	0.001	0.001	0.000	0.000

The number of Automatic Tie Points (ATPs) per pixel averaged over all images of the camera model is color coded between black and white. White indicates that, in average, more than 16 ATPs are extracted at this pixel location. Black indicates that, in average, 0 ATP has been extracted at this pixel location. Click on the image to see the average direction and magnitude of the reprojection error for each pixel. Note that the vectors are scaled for better visualization.

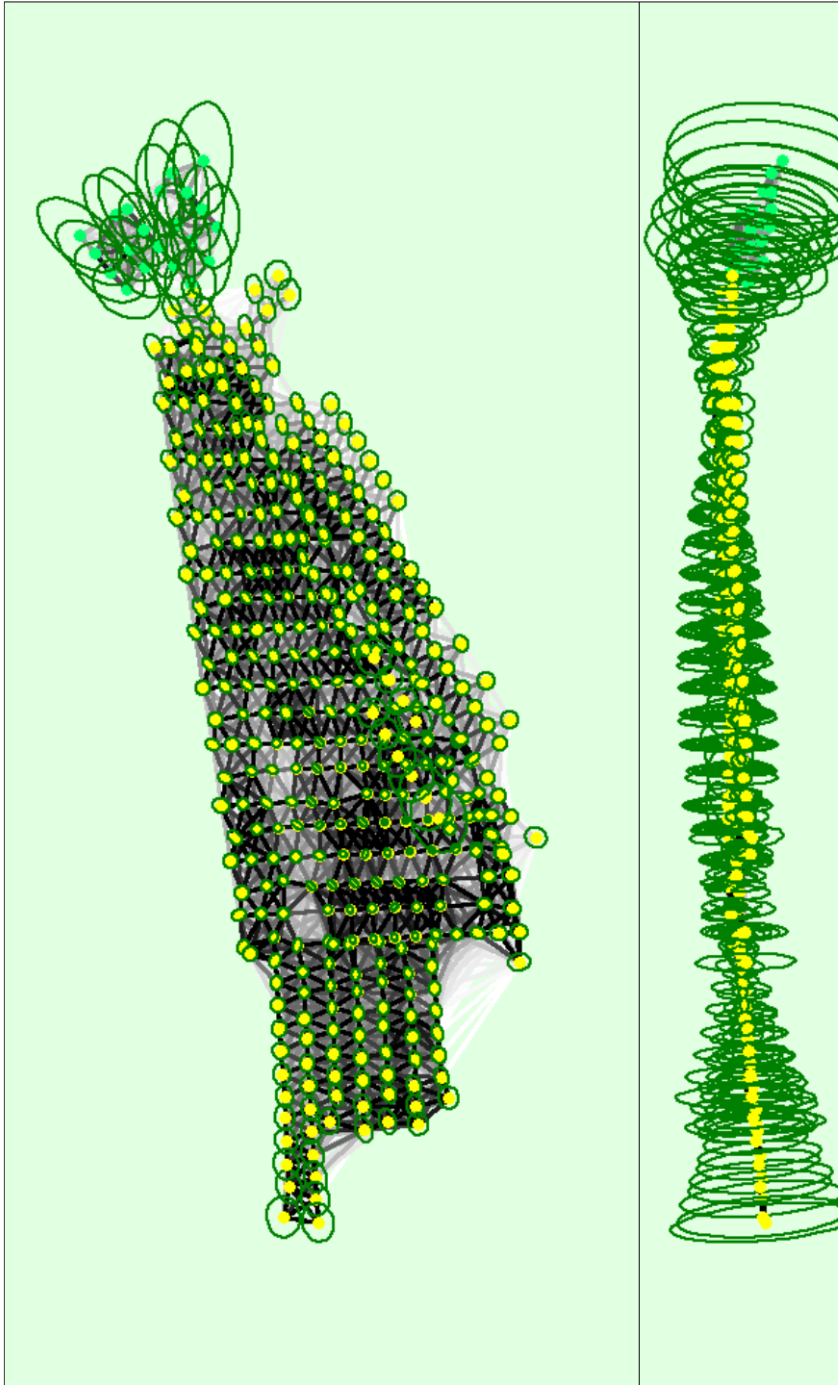
2D Keypoints Table

	Number of 2D Keypoints per Image	Number of Matched 2D Keypoints per Image
Median	33187	12796
Min	18735	1443
Max	57647	21771
Mean	32661	12658

3D Points from 2D Keypoint Matches

	Number of 3D Points Observed
In 2 Images	1261521
In 3 Images	318589
In 4 Images	127382
In 5 Images	64946
In 6 Images	36505
In 7 Images	21972
In 8 Images	14143
In 9 Images	8879
In 10 Images	4713
In 11 Images	2715
In 12 Images	1473
In 13 Images	668
In 14 Images	232
In 15 Images	75
In 16 Images	29
In 17 Images	9

🔍 2D Keypoint Matches



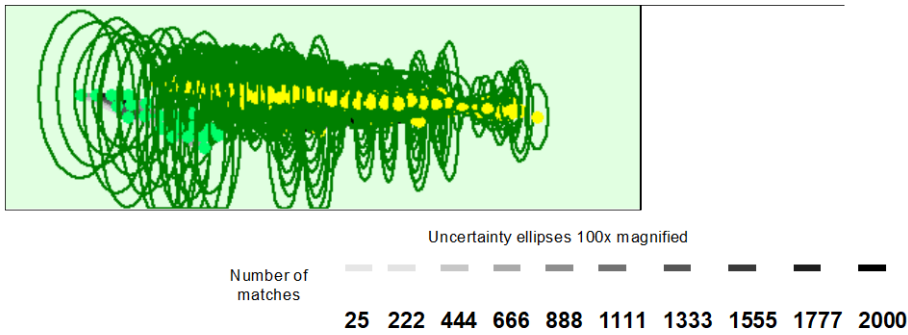


Figure 5: Computed image positions with links between matched images. The darkness of the links indicates the number of matched 2D keypoints between the images. Bright links indicate weak links and require manual tie points or more images. Dark green ellipses indicate the relative camera position uncertainty of the bundle block adjustment result.

Relative camera position and orientation uncertainties

	X [m]	Y [m]	Z [m]	Omega [degree]	Phi [degree]	Kappa [degree]
Mean	0.020	0.025	0.071	0.131	0.121	0.036
Sigma	0.014	0.020	0.050	0.064	0.068	0.030

Manual Tie Points

MTP Name	Projection Error [pixel]	Verified/Marked
mtp1	0.460	10 / 10
mtp2	0.263	10 / 10
mtp3	0.888	4 / 4
mtp4	0.490	5 / 5
mtp5	0.562	4 / 4
mtp6	1.207	8 / 8
mtp7	1.336	11 / 11
mtp8	1.004	13 / 13
mtp9	1.410	8 / 8

Projection errors for manual tie points. The last column counts the number of images where the manual tie point has been automatically verified vs. manually marked.

Geolocation Details

Ground Control Points

GCP Name	Accuracy XY/Z [m]	Error X [m]	Error Y [m]	Error Z [m]	Projection Error [pixel]	Verified/Marked
0 (3D)	0.020/ 0.020	-0.008	0.002	-0.000	0.750	9 / 9
1 (3D)	0.020/ 0.020	0.003	0.002	0.000	0.678	7 / 7
2 (3D)	0.020/ 0.020	0.004	-0.004	0.000	0.452	10 / 10
Mean [m]		-0.000002	-0.000003	0.000001		
Sigma [m]		0.005528	0.003110	0.000044		
RMS Error [m]		0.005528	0.003110	0.000044		

Localisation accuracy per GCP and mean errors in the three coordinate directions. The last column counts the number of calibrated images where the GCP has been automatically verified vs. manually marked.

🔍 Absolute Geolocation Variance



Min Error [m]	Max Error [m]	Geolocation Error X [%]	Geolocation Error Y [%]	Geolocation Error Z [%]
-	-15.00	0.00	0.00	0.00
-15.00	-12.00	0.00	0.00	0.00
-12.00	-9.00	0.00	0.00	0.00
-9.00	-6.00	6.09	0.00	1.02
-6.00	-3.00	8.88	0.00	6.60
-3.00	0.00	10.66	62.44	44.42
0.00	3.00	70.05	36.55	36.29
3.00	6.00	4.06	1.02	11.17
6.00	9.00	0.00	0.00	0.51
9.00	12.00	0.25	0.00	0.00
12.00	15.00	0.00	0.00	0.00
15.00	-	0.00	0.00	0.00
Mean [m]		-0.219628	0.508503	-0.071659
Sigma [m]		2.745964	0.977126	2.366377
RMS Error [m]		2.754733	1.101522	2.367462

Min Error and Max Error represent geolocation error intervals between -1.5 and 1.5 times the maximum accuracy of all the images. Columns X, Y, Z show the percentage of images with geolocation errors within the predefined error intervals. The geolocation error is the difference between the initial and computed image positions. Note that the image geolocation errors do not correspond to the accuracy of the observed 3D points.

Geolocation Bias	X	Y	Z
Translation [m]	-0.219628	0.508503	-0.071659

Bias between image initial and computed geolocation given in output coordinate system.

🔍 Relative Geolocation Variance



Relative Geolocation Error	Images X [%]	Images Y [%]	Images Z [%]
[-1.00, 1.00]	88.58	100.00	100.00
[-2.00, 2.00]	100.00	100.00	100.00
[-3.00, 3.00]	100.00	100.00	100.00
Mean of Geolocation Accuracy [m]	5.000000	5.000000	10.000000
Sigma of Geolocation Accuracy [m]	0.000000	0.000000	0.000000

Images X, Y, Z represent the percentage of images with a relative geolocation error in X, Y, Z.

Geolocation Orientational Variance	RMS [degree]
Omega	4.848
Phi	4.033
Kappa	7.242

Geolocation RMS error of the orientation angles given by the difference between the initial and computed image orientation angles.

Initial Processing Details



System Information



Hardware	CPU: Intel(R) Core(TM) i7-7820HQ CPU @ 2.90GHz RAM: 16GB GPU: no info (Driver: unknown)
Operating System	Darwin 18.6.0 x86_64

Coordinate Systems i

Image Coordinate System	WGS84 (egm96)
Ground Control Point (GCP) Coordinate System	WGS84 / UTM zone 32N (egm96)
Output Coordinate System	WGS84 / UTM zone 32N (egm96)

Processing Options i

Detected Template	 3D Maps
Keypoints Image Scale	Full, Image Scale: 1
Advanced: Matching Image Pairs	Aerial Grid or Corridor
Advanced: Matching Strategy	Use Geometrically Verified Matching: no
Advanced: Keypoint Extraction	Targeted Number of Keypoints: Automatic
Advanced: Calibration	Calibration Method: Standard Internal Parameters Optimization: All External Parameters Optimization: All Rematch: Auto, yes Bundle Adjustment: Classic

DSM, Orthomosaic and Index Details i

Processing Options i

DSM and Orthomosaic Resolution	1 x GSD (0.57 [cm/pixel])
DSM Filters	Noise Filtering: yes Surface Smoothing: yes, Type: Sharp
Raster DSM	Generated: yes Method: Inverse Distance Weighting Merge Tiles: yes
Orthomosaic	Generated: yes Merge Tiles: yes GeoTIFF Without Transparency: no Google Maps Tiles and KML: no
Time for DSM Generation	16m:38s
Time for Orthomosaic Generation	32m:31s

Appendix D: German School Parking Lot; Pix4D Quality Report

Quality Report



Generated with Pix4Dmapper Pro version 3.0.18

! **Important:** Click on the different icons for:

- ?** Help to analyze the results in the Quality Report
- i** Additional information about the sections

💡 Click [here](#) for additional tips to analyze the Quality Report

Summary



Project	gisp_studysite2
Processed	2019-05-29 21:47:39
Camera Model Name(s)	FC330_3.6_4000x3000 (RGB)
Average Ground Sampling Distance (GSD)	0.62 cm / 0.24 in
Area Covered	0.0091 km ² / 0.9149 ha / 0.0035 sq. mi. / 2.2619 acres
Time for Initial Processing (without report)	45m:02s

Quality Check



? Images	median of 18049 keypoints per image	✔
? Dataset	452 out of 454 images calibrated (99%), all images enabled	✔
? Camera Optimization	3.64% relative difference between initial and optimized internal camera parameters	✔
? Matching	median of 3520.87 matches per calibrated image	✔
? Georeferencing	yes, 4 GCPs (4 3D), mean RMS error = 0.028 m	⚠

Preview

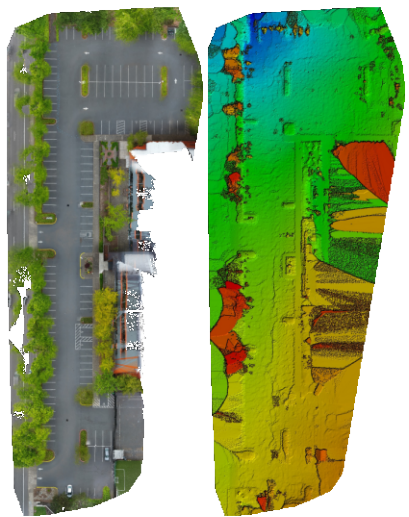


Figure 1: Orthomosaic and the corresponding sparse Digital Surface Model (DSM) before densification.

Calibration Details

Number of Calibrated Images	452 out of 454
Number of Geolocated Images	454 out of 454

Initial Image Positions

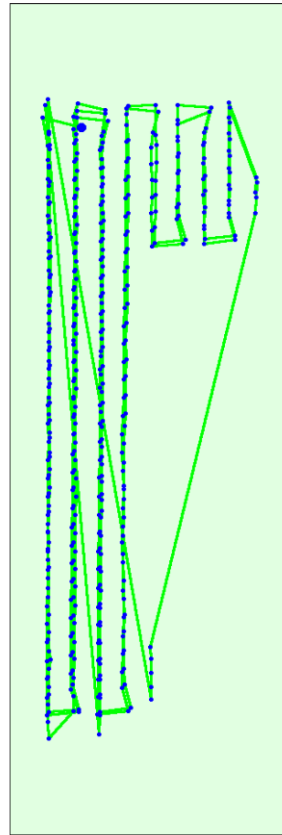
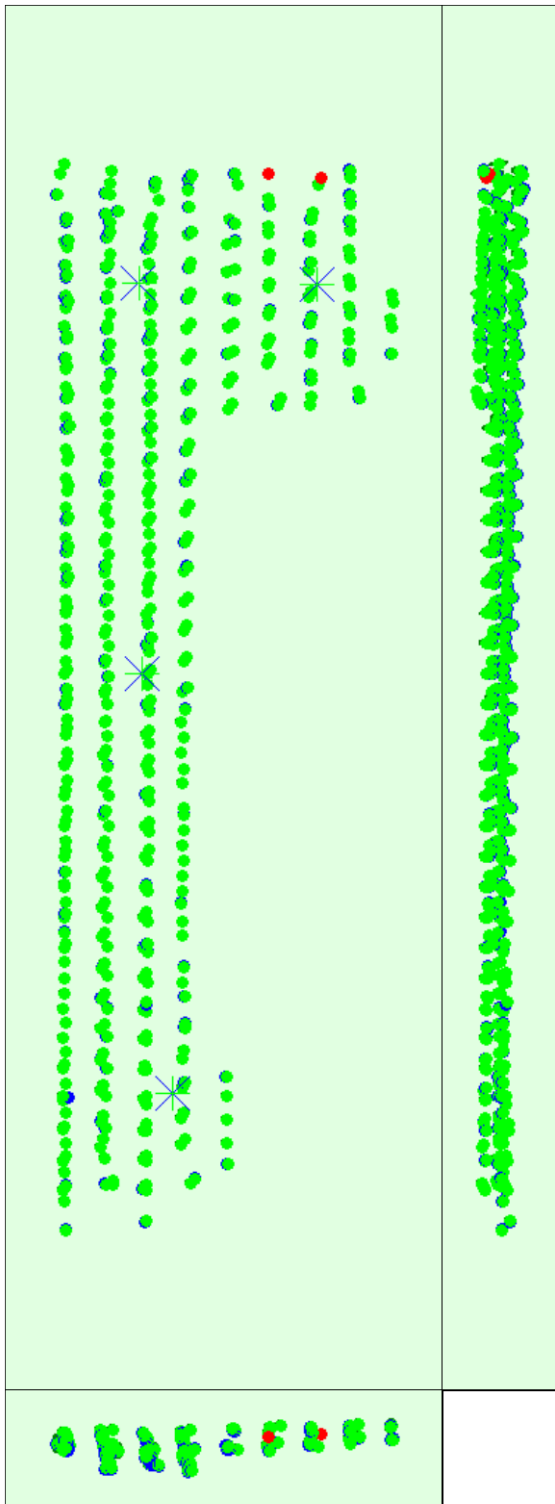


Figure 2: Top view of the initial image position. The green line follows the position of the images in time starting from the large blue dot.

Computed Image/GCPs/Manual Tie Points Positions



Uncertainty ellipses 1x magnified

Figure 3: Offset between initial (blue dots) and computed (green dots) image positions as well as the offset between the GCPs initial positions (blue crosses) and their computed positions (green crosses) in the top-view (XY plane), front-view (XZ plane), and side-view (YZ plane). Red dots indicate disabled or uncalibrated images. Dark

green ellipses indicate the absolute position uncertainty of the bundle block adjustment result.

🔍 Absolute camera position and orientation uncertainties i

	X [m]	Y [m]	Z [m]	Omega [degree]	Phi [degree]	Kappa [degree]
Mean	0.547	0.322	0.640	0.694	1.610	0.248
Sigma	0.053	0.053	0.179	0.313	0.149	0.028

🔍 Overlap i

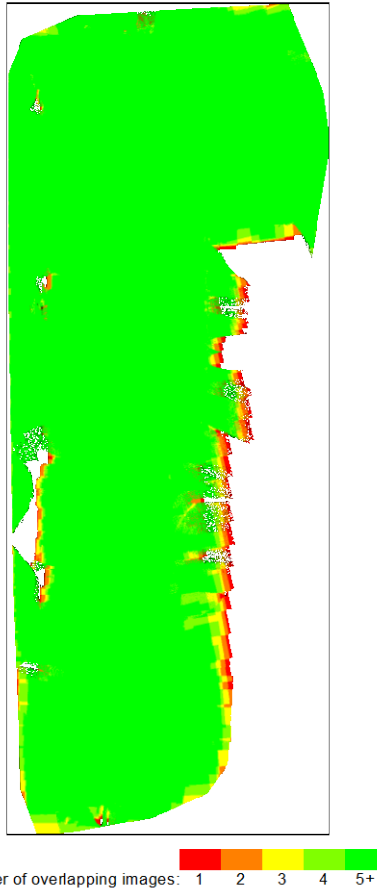


Figure 4: Number of overlapping images computed for each pixel of the orthomosaic. Red and yellow areas indicate low overlap for which poor results may be generated. Green areas indicate an overlap of over 5 images for every pixel. Good quality results will be generated as long as the number of keypoint matches is also sufficient for these areas (see Figure 5 for keypoint matches).

Bundle Block Adjustment Details i

Number of 2D Keypoint Observations for Bundle Block Adjustment	1709242
Number of 3D Points for Bundle Block Adjustment	555378
Mean Reprojection Error [pixels]	0.210

Internal Camera Parameters

FC330_3.6_4000x3000 (RGB). Sensor Dimensions: 6.317 [mm] x 4.738 [mm]

EXIF ID: FC330_3.6_4000x3000

	Focal Length	Principal Point x	Principal Point y	R1	R2	R3	T1	T2
Initial Values	2285.722 [pixel] 3.610 [mm]	2000.006 [pixel] 3.159 [mm]	1500.003 [pixel] 2.369 [mm]	-0.001	-0.002	0.000	-0.001	-0.001
Optimized Values	2369.123 [pixel] 3.742 [mm]	2006.685 [pixel] 3.169 [mm]	1514.178 [pixel] 2.391 [mm]	0.003	-0.010	0.004	-0.000	0.000
Uncertainties (Sigma)	4.230 [pixel] 0.007 [mm]	0.483 [pixel] 0.001 [mm]	0.269 [pixel] 0.000 [mm]	0.000	0.001	0.001	0.000	0.000



The number of Automatic Tie Points (ATPs) per pixel averaged over all images of the camera model is color coded between black and white. White indicates that, in average, more than 16 ATPs are extracted at this pixel location. Black indicates that, in average, 0 ATP has been extracted at this pixel location. Click on the image to see the average direction and magnitude of the reprojection error for each pixel. Note that the vectors are scaled for better visualization.

2D Keypoints Table

	Number of 2D Keypoints per Image	Number of Matched 2D Keypoints per Image
Median	18049	3521
Min	15081	445
Max	58351	9893
Mean	22041	3782

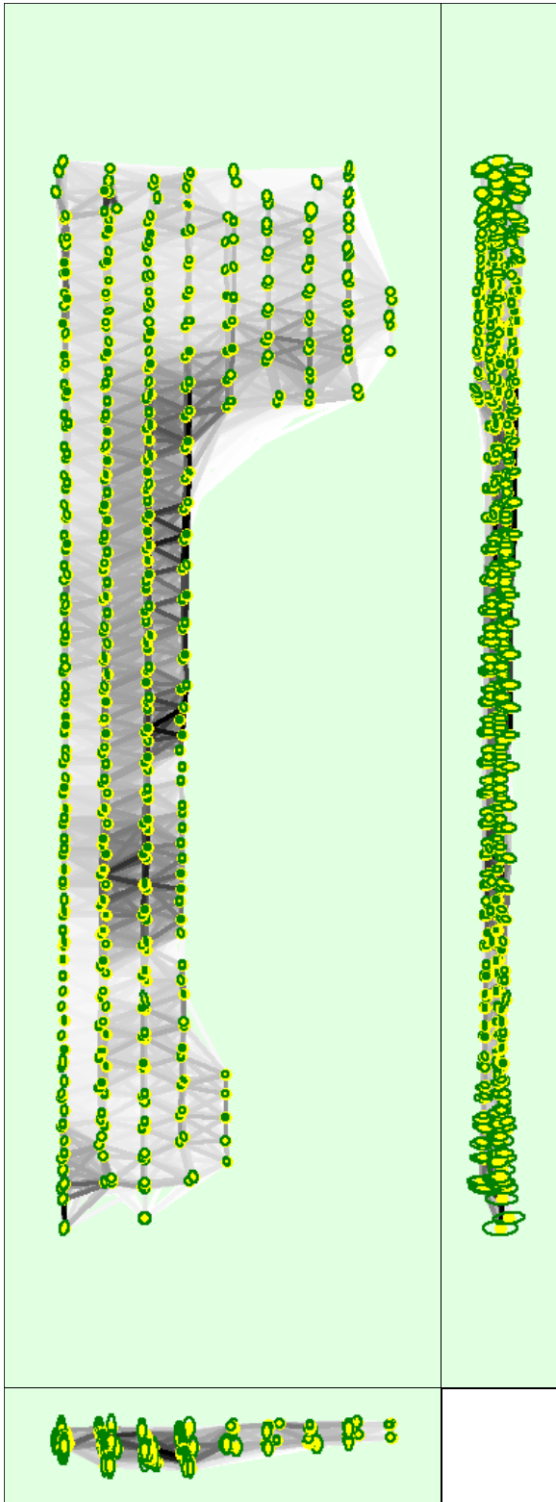
3D Points from 2D Keypoint Matches

	Number of 3D Points Observed
In 2 Images	374311
In 3 Images	80538
In 4 Images	34335
In 5 Images	18732
In 6 Images	11903
In 7 Images	7904
In 8 Images	5659
In 9 Images	4071
In 10 Images	3218
In 11 Images	2462
In 12 Images	2101
In 13 Images	1549
In 14 Images	1284
In 15 Images	1071
In 16 Images	899
In 17 Images	743
In 18 Images	578
In 19 Images	527
In 20 Images	479
In 21 Images	373
In 22 Images	315
In 23 Images	294

In 24 Images	277
In 25 Images	188
In 26 Images	208
In 27 Images	142
In 28 Images	133
In 29 Images	108
In 30 Images	128
In 31 Images	106
In 32 Images	100
In 33 Images	87
In 34 Images	106
In 35 Images	74
In 36 Images	58
In 37 Images	53
In 38 Images	39
In 39 Images	40
In 40 Images	21
In 41 Images	26
In 42 Images	32
In 43 Images	19
In 44 Images	12
In 45 Images	14
In 46 Images	9
In 47 Images	16
In 48 Images	11
In 49 Images	6
In 50 Images	5
In 51 Images	3
In 52 Images	2
In 53 Images	1
In 54 Images	2
In 55 Images	1
In 57 Images	1
In 59 Images	2
In 60 Images	1
In 61 Images	1

 2D Keypoint Matches





Uncertainty ellipses 50x magnified

Number of matches



Figure 5: Computed image positions with links between matched images. The darkness of the links indicates the number of matched 2D keypoints between the images. Bright links indicate weak links and require manual tie points or more images. Dark green ellipses indicate the relative camera position uncertainty of the bundle block adjustment result.

Relative camera position and orientation uncertainties

	X [m]	Y [m]	Z [m]	Omega [degree]	Phi [degree]	Kappa [degree]
Mean	0.010	0.012	0.017	0.060	0.038	0.020
Sigma	0.002	0.002	0.009	0.021	0.009	0.006

Geolocation Details

Ground Control Points

GCP Name	Accuracy XY/Z [m]	Error X [m]	Error Y [m]	Error Z [m]	Projection Error [pixel]	Verified/Marked
1 (3D)	0.690/ 0.870	-0.020	-0.006	0.001	0.416	27 / 27
2 (3D)	0.770/ 0.930	0.030	0.021	-0.053	0.378	41 / 41
3 (3D)	0.740/ 1.000	0.033	-0.002	-0.033	0.693	46 / 46
4 (3D)	0.640/ 0.860	-0.028	-0.008	0.068	0.544	57 / 57
Mean [m]		0.003699	0.001271	-0.004069		
Sigma [m]		0.028044	0.011440	0.046045		
RMS Error [m]		0.028287	0.011510	0.046225		

Localisation accuracy per GCP and mean errors in the three coordinate directions. The last column counts the number of calibrated images where the GCP has been automatically verified vs. manually marked.

Absolute Geolocation Variance

Min Error [m]	Max Error [m]	Geolocation Error X [%]	Geolocation Error Y [%]	Geolocation Error Z [%]
-	-7.50	0.00	0.00	0.00
-7.50	-6.00	0.00	0.00	0.00
-6.00	-4.50	0.00	0.00	0.00
-4.50	-3.00	0.00	0.00	0.00
-3.00	-1.50	0.00	0.00	0.00
-1.50	0.00	44.69	47.12	56.42
0.00	1.50	55.31	52.88	43.58
1.50	3.00	0.00	0.00	0.00
3.00	4.50	0.00	0.00	0.00
4.50	6.00	0.00	0.00	0.00
6.00	7.50	0.00	0.00	0.00
7.50	-	0.00	0.00	0.00
Mean [m]		-0.050026	0.011861	-0.104742
Sigma [m]		0.055738	0.023694	0.091920
RMS Error [m]		0.074895	0.026497	0.139356

Min Error and Max Error represent geolocation error intervals between -1.5 and 1.5 times the maximum accuracy of all the images. Columns X, Y, Z show the percentage of images with geolocation errors within the predefined error intervals. The geolocation error is the difference between the initial and computed image positions. Note

that the image geolocation errors do not correspond to the accuracy of the observed 3D points.

Geolocation Bias	X	Y	Z
Translation [m]	-0.050026	0.011861	-0.104742

Bias between image initial and computed geolocation given in output coordinate systems.

Relative Geolocation Variance

Relative Geolocation Error	Images X [%]	Images Y [%]	Images Z [%]
[-1.00, 1.00]	100.00	100.00	100.00
[-2.00, 2.00]	100.00	100.00	100.00
[-3.00, 3.00]	100.00	100.00	100.00
Mean of Geolocation Accuracy [m]	5.000000	5.000000	5.000000
Sigma of Geolocation Accuracy [m]	0.000000	0.000000	0.000000

Images X, Y, Z represent the percentage of images with a relative geolocation error in X, Y, Z.

Geolocation Orientational Variance	RMS [degree]
Omega	1.522
Phi	4.678
Kappa	8.801

Geolocation RMS error of the orientation angles given by the difference between the initial and computed image orientation angles.

Initial Processing Details

System Information

Hardware	CPU: Intel(R) Core(TM) i7-7820HQ CPU @ 2.90GHz RAM: 16GB GPU: no info (Driver: unknown)
Operating System	Darwin 18.6.0 x86_64

Coordinate Systems

Image Coordinate System	WGS 84 / UTM zone 10N (egm96)
Ground Control Point (GCP) Coordinate System	WGS 84 / UTM zone 10N (2D)
Output Coordinate System	WGS 84 / UTM zone 10N (2D)

Processing Options

Detected Template	3D Maps
Keypoints Image Scale	Full, Image Scale: 1
Advanced: Matching Image Pairs	Aerial Grid or Corridor
Advanced: Matching Strategy	Use Geometrically Verified Matching: no
Advanced: Keypoint Extraction	Targeted Number of Keypoints: Automatic
Advanced: Calibration	Calibration Method: Standard Internal Parameters Optimization: All External Parameters Optimization: All Rematch: Auto, yes Bundle Adjustment: Classic

DSM, Orthomosaic and Index Details



Processing Options



DSM and Orthomosaic Resolution	1 x GSD (0.626 [cm/pixel])
DSM Filters	Noise Filtering: yes Surface Smoothing: yes, Type: Sharp
Raster DSM	Generated: yes Method: Inverse Distance Weighting Merge Tiles: yes
Orthomosaic	Generated: yes Merge Tiles: yes GeoTIFF Without Transparency: no Google Maps Tiles and KML: no
Time for DSM Generation	07m:08s
Time for Orthomosaic Generation	29m:56s